



UNIVERSITY OF LEEDS

This is a repository copy of *Testing models of ice cap extent, South Georgia, sub-Antarctic*.

White Rose Research Online URL for this paper:

<http://eprints.whiterose.ac.uk/107105/>

Version: Accepted Version

---

**Article:**

Barlow, NLM [orcid.org/0000-0002-2713-2543](http://orcid.org/0000-0002-2713-2543), Bentley, MJ, Spada, G et al. (6 more authors) (2016) Testing models of ice cap extent, South Georgia, sub-Antarctic. *Quaternary Science Reviews*, 154. pp. 157-168. ISSN 0277-3791

<https://doi.org/10.1016/j.quascirev.2016.11.007>

---

© 2016, Elsevier. Licensed under the Creative Commons Attribution-NonCommercial-NoDerivatives 4.0 International <http://creativecommons.org/licenses/by-nc-nd/4.0/>

**Reuse**

Unless indicated otherwise, fulltext items are protected by copyright with all rights reserved. The copyright exception in section 29 of the Copyright, Designs and Patents Act 1988 allows the making of a single copy solely for the purpose of non-commercial research or private study within the limits of fair dealing. The publisher or other rights-holder may allow further reproduction and re-use of this version - refer to the White Rose Research Online record for this item. Where records identify the publisher as the copyright holder, users can verify any specific terms of use on the publisher's website.

**Takedown**

If you consider content in White Rose Research Online to be in breach of UK law, please notify us by emailing [eprints@whiterose.ac.uk](mailto:eprints@whiterose.ac.uk) including the URL of the record and the reason for the withdrawal request.



[eprints@whiterose.ac.uk](mailto:eprints@whiterose.ac.uk)  
<https://eprints.whiterose.ac.uk/>

## Testing models of ice cap extent, South Georgia, sub-Antarctic.

Barlow, N.L.M.<sup>1,2\*</sup>, Bentley, M.J.<sup>1</sup>, Spada, G.<sup>3</sup>, Evans, D.J.A.<sup>1</sup>, Hansom, J.D.<sup>4</sup>, Brader, M.D.<sup>1</sup>, White, D.A.<sup>5</sup>, Zander, A.<sup>6</sup>, Berg, S.<sup>7</sup>

<sup>1</sup> Department of Geography, Durham University, South Road, Durham, DH1 3LE, UK

<sup>2</sup> School of Earth and Environment, University of Leeds, Leeds, LS2 9JT, UK

<sup>3</sup> Dipartimento di Scienze Pure e Applicate (DiSPeA) Urbino University "Carlo Bo", Urbino, Italy

<sup>4</sup> School of Geographical and Earth Sciences, University of Glasgow, Glasgow, G12 8QQ, UK

<sup>5</sup> Institute for Applied Ecology, University of Canberra, Canberra, ACT 2617, Australia.

<sup>6</sup> Institute of Geography, University of Cologne, Albertus-Magnus-Platz, 50923 Cologne, Germany

<sup>7</sup> Institute of Geology and Mineralogy, University of Cologne, Zùlpicher Str. 49a, 50674 Cologne, Germany

\* Corresponding author: [n.l.m.barlow@leeds.ac.uk](mailto:n.l.m.barlow@leeds.ac.uk) +44 113 343 3761

### Keywords

Last Glacial Maximum, glacial isostatic adjustment, sea-level change, South Georgia, sub-Antarctic, coastal geomorphology

## **Abstract**

The extent of Last Glacial Maximum ice in South Georgia is contested, with two alternative hypotheses: an extensive (maximum) model of ice reaching the edge of the continental shelf, or a restricted (minimum) model with ice constrained within the inner fjords. We present a new relative sea-level dataset for South Georgia, summarising published and new geomorphological evidence for the marine limit and elevations of former sea levels on the island. Using a glacial isostatic adjustment model (ALMA) specifically suited to regional modelling and working at high spatial resolutions, combined with a series of simulated ice-load histories, we use the relative sea-level data to test between the restricted and extensive ice extent scenarios. The model results suggest that there was most likely an extensive Last Glacial Maximum glaciation of South Georgia, implying that the island was covered by thick (>1000 m) ice, probably to the edge of the continental shelf, with deglaciation occurring relatively early (ca. 15 ka BP, though independent data suggest this may have been as early as 18 ka). The presence of an extensive ice cap extending to the shelf edge would imply that if there were any biological refugia around South Georgia, they must have been relatively localised and restricted to the outermost shelf.

## **Rationale and background**

Though limited in size, the extent of glaciations of the sub-Antarctic islands, such as South Georgia, is of considerable interest due to their position in the Southern Ocean, providing a potential link between the climates of South America and West Antarctica (Hall, 2009; Hodgson et al., 2014a; 2014b). Moreover, the extent of ice has important implications as to whether the sub-Antarctic islands acted as glacial refugia for biota (Barnes et al., 2006; Barnes et al., 2016; Hodgson et al., 2014b; Hogg et al., 2011; Thatje et al., 2008). Though the contribution of the potential ice mass on South Georgia to global sea level will be modest, recent changes in glacier extent in response to 20<sup>th</sup> century warming (Cook et al., 2010; Gordon et al., 2008) demonstrates the sensitivity of maritime South Georgia to changes in climate and oceanographic forcing by the Southern Ocean. During the global Last Glacial Maximum (LGM), ice on South Georgia expanded (Bentley et al., 2007; Hodgson et al., 2014b; Sugden and Clapperton, 1977) but there remains significant debate about the maximum ice extent reached during this time. Two widely divergent models have been suggested for the size of the ice cap over South Georgia during the LGM: an extensive (maximum) model of ice reaching the edge of the continental shelf (during at least one glacial phase) (Sugden and Clapperton, 1977), or a restricted (minimum) model with ice being constrained within the inner fjords (Bentley et al., 2007). The aim of this paper is to use glacial-isostatic adjustment (GIA) modelling in association with geomorphological evidence of former marine limits and past sea levels, as a means to test between the alternative models of former ice cap extent on South Georgia.

### *The maximum model*

The maximum model was suggested by Sugden and Clapperton (1977), based on the undulating and glacially scoured morphology of the continental shelf and the deep glacial troughs incised into it. They used precision depth recorder data to suggest that whereas the troughs are offshore extensions of fjords containing many features characteristic of glacier erosion, the areas between the troughs are characterised by irregular topography of the order of 20-80 m of relief. They argued that these

features are uncommon on 'normal' continental shelves where sediment deposition tends to obscure irregular relief. Based upon the limited offshore data available, they documented evidence for glacial areal scour almost everywhere on the shelf shallower than 200 m and estimate a maximum ice area of 30,000 km<sup>2</sup>. Sugden and Clapperton (1977) suggested that this extensive shelf-extent glaciation must have predated the last island-wide glaciation of South Georgia based upon preserved beach material emplaced on land between two periods of glacial sedimentation.

New bathymetric data, including swath bathymetry of some key areas, led Graham et al. (2008) to suggest an extensive ice cap at the LGM but acknowledged that there was little dating evidence to support this. Their evidence included more detailed mapping of the troughs noted by Sugden and Clapperton (1977), as well as the discovery of submarine landforms interpreted as moraines, located in the troughs close to the shelf edge (Figure 1).

#### *The minimum model*

A minimum model for ice cap glaciation was suggested by Bentley et al. (2007) based on dated onshore geomorphological evidence mapped across a variety of fjords along the north-east coast of South Georgia. In particular, Bentley et al. (2007) mapped a consistent pattern of moraines that did not extend beyond the fjord mouths, and dated these using cosmogenic nuclide surface exposure dating. They also noted the low elevation (<10 m) of all post-glacial raised beaches, implying a minor amount of glacial isostatic rebound and a relatively small antecedent ice cap. Based on the geomorphology and cosmogenic exposure ages, and a well-dated lake sediment core implying ice-free inner fjords as early as 18,621–19,329 cal yr BP at the Tønsberg Peninsula (Rosqvist et al., 1999), Bentley et al. (2007) suggested that the ice did not extend beyond the fjord mouths at the LGM. Direct observations of recent behaviour of South Georgia glaciers has identified precipitation as the primary controlling factor on tidewater glaciers (Gordon and Timmis, 1992) and using this analogue Bentley et al. (2007)

suggested that the restricted extent of LGM glaciation may have been due to low precipitation caused by extensive sea ice presence upwind of South Georgia.

Hodgson et al. (2014a) used multibeam swath bathymetric surveys of nine major fjords around South Georgia to reveal a relatively consistent pattern of submarine geomorphological features. These include a shallow inner basin bounded by an inner basin moraine and a deep basin with a moraine at the outer limits of each of the fjords. Using a relative chronology based primarily on existing terrestrial evidence from Bentley et al. (2007), they suggested that the inner basin moraines date from the last major glacial advance (LGM), and the deep basin moraines from an earlier glaciation, possibly marine isotope stage (MIS) 6. However, they suggested offshore marine work is required to date the deglacial morainic sediments.

#### *Timing of post-LGM deglaciation*

Numerous studies have sought to date the timing of deglaciation on South Georgia using terrestrial proxies for ice retreat, of which Hodgson et al. (2014b) provide a comprehensive review. To date, the offshore evidence is limited to bathymetric surveys with little direct chronological control. The onshore oldest cosmogenic isotope dates mark the oldest mapped ice advance, estimated using an error-weighted mean to have been abandoned at  $12.1 \pm 1.4$  yr BP (Bentley et al., 2007). The oldest evidence for post LGM ice-free conditions comes from the radiocarbon dates marking the onset of lake sedimentation in one basin on the Tønsberg Peninsula, close to Husvik, at 18,621–19,329 cal yr BP (Rosqvist et al., 1999). Most other basal dates from lake sediments and peat sequences provide minimum ages for ice-free conditions from the start of the Holocene (Table 1 in Hodgson et al., 2014b).

To test the two differing hypothesis of extensive (maximum) or restricted (minimum) ice limits during the LGM we develop two sets of ice models that simulate extensive (shelf based) or restricted (island only) glaciation that we input into a GIA model, the outputs of which we compare to the

geomorphological evidence of former relative sea levels (RSL) from the island. The results have implications for understanding of sub-Antarctic glaciation, ongoing patterns of land-level displacement and the climate of the Southern Ocean.

### **Study area**

South Georgia is 170 km long and its width varies from 2 to 40 km (Figure 1). It is dominated by a central spine of mountains rising to nearly 3000 m (Mount Paget is the highest peak at 2935 m). The axis of the island hosts a series of linked icefields from which numerous outlet glaciers descend. Most terminate as tidewater fronts but a few have terrestrial margins. The glaciers have eroded deep fjords that dominate the South Georgia coastline and at the head of most of these is a large outlet glacier. South Georgia currently has a cool climate (mean annual temperature 2°C) with a strong maritime influence (Smith, 1960). The regional equilibrium line altitude (ELA) on the north-east of the island was estimated by Smith (1960) to be 460 m above sea level (asl). Much of the data reported here is focused on the north-east coast of the island where there are several ice-free peninsulas between the fjords which can be logistically accessed, and on which is located a rich geomorphological record of glacial landforms and raised coastal features (Bentley et al., 2007; Clapperton et al., 1989; Stone, 1974; Sugden and Clapperton, 1977). The south-west coast is data-poor since it is largely glaciated down to sea level, difficult to access, and has limited present and raised marine features (Hansom, 1979).

### **Field data**

To test the hypothesis of extensive versus restricted ice extent during the LGM we compiled a dataset of geomorphological evidence of the elevation of past sea level (Figures 1, 2 and 3), to compare against the GIA model outputs. There is widespread and consistent evidence of the postglacial marine limit on South Georgia and a small number of dated sea-level index points.

### *Raised marine features*

There is a wide range of raised marine features around the island, most of which have been identified along the north-east coastline where previous work and our own mapping has focussed (Figure 1, Tables 1 and 2). These can be divided into two main groups: raised beaches and rock platforms. The raised beaches consist of an assemblage of common landforms that are always found below 10 m asl, though are found above modern beach level either due to relative sea-level fall and/or long-term tectonic uplift (Figures 1 and 2). They typically consist of raised gravel beaches and terraces cut into existing glacial or slope deposits (e.g. Gordon and Hansom, 1986). The deposits are usually crudely bedded gravels, small boulders and coarse sand, with subhorizontal layering. Most of these are not directly dated. There are also a small number of landforms <10 m asl such as isolation basins, and a dune complex that have allowed us to provide dated constraints on relative sea-level change. We identify these low elevation features as post-LGM in age based on the following characteristics: fresh appearance of sediments, lack of overlying glacial or slope sediments and cross-cutting relationships with moraine deposits located in the fjords, as well as a small number of direct ages on selected landforms (Table 1). We surveyed many of these beaches to add to the raised gravel beaches surveyed by Stone (1974, 1976), and sequences of raised beaches at 2-4 m and 6-10 m noted by Hansom (1979) and Clapperton et al. (1989).

The second set of landforms consists of rock platforms, mostly located at present sea level and between 20 and 50 m asl. These comprise prominent terraces backed by a cliff, usually cut into bedrock, or occasionally surficial sediments, and are frequently consistent in elevation across sets of adjacent headlands (Adie, 1964; Stone, 1974). The platforms have been discussed since Gregory (1915) interpreted them as 'a wide plain of marine denudation', and have been reported as high as 150 m asl although few of the platforms >50 m have been unequivocally ascribed a marine origin (Stone, 1974). The rock platforms around the island are usually capped by erratics and till and so pre-date the last glaciation, especially as they extend under the most recent fjord and valley side moraines

around the island (Bentley et al., 2007). For this reason we do not use them for directly constraining the GIA model output of post-glacial RSL change but they are useful for understanding the long-term landscape evolution of the island.

Clapperton (1971), Sugden and Clapperton (1977) and Clapperton et al. (1989) also noted the presence of older raised beaches at higher elevations than the post-LGM beaches. These are identified as older than post-LGM because they are partly lithified and cemented with iron oxide, and the well-rounded clasts of some are covered by, and incorporated into, till (Clapperton et al., 1989; Clapperton et al., 1978). They include examples in Kelp Bay (at 20m asl) and Harcourt Foreland the north side of Royal Bay (at 52m asl) (Sugden and Clapperton, 1977), and six other unnamed sites that occur up to 40 m asl along the south coast of the island (Clapperton et al., 1989). We therefore constrain the postglacial marine limit to be below 10 m asl with no evidence for post-LGM marine features above this elevation.

#### *Dated constraints on relative sea-level change*

Clapperton et al. (1978) showed that the highest beach they recorded in St Andrews Bay (6-7.2 m) was cut into a moraine and therefore formed after deglaciation from that moraine. Dates on the lowermost layer of peat accumulated on top of the till of the equivalent moraine in King Edward Cove yielded a radiocarbon age of  $9493 \pm 370$   $^{14}\text{C}$  yr BP (SRR-736), which thus provides a minimum age for the moraine. The beach was covered by a layer of peat which yielded a basal age of  $3997 \pm 85$   $^{14}\text{C}$  yr BP (SRR-597). Clapperton et al. (1978) therefore concluded that the highest beach was formed sometime between 9500 and 4000  $^{14}\text{C}$  yr BP (equivalent to a calibrated age between 9677–11832 and 4148-4645 cal yr BP). Calculating the indicative range of a raised marine beach is a challenge (Kelsey, 2015) and therefore we use the ages from Clapperton et al. (1978) in Figure 3 to constrain the potential maximum and minimum ages for this feature, but apply a more conservative 6-10 m range for the marine limit based upon the range of mapped elevations (Figure 1).

Stone (1979) reported a site on the south side of Royal Bay where a series of raised beaches at 6 m asl extends into a sea-cave system. A fibrous mat of organic sediment including moulted seal skin and hair yielded a radiocarbon age of  $2369 \pm 40$   $^{14}\text{C}$  yr BP (SRR-520). This provides a minimum age for the 6m raised beach found at the back of the cave (Stone, 1979).

In Enten Valley the raised beaches are covered by a sequence of beach foredunes and shadow dunes where at least seven large beach ridges (E1-7), and several smaller ridges are preserved across a 400 m wide strandplain (Figure 4 and supplementary information). Most of the inland dune sands are indurated and covered by a thin (0.1-0.3 m) layer of peat, with soil and peat thicknesses generally increasing inland, suggesting increasing age. Peat accumulations on the dunes are substantially thinner than on the nearby (near sea level) moraines, which are commonly covered by over a metre of peat, suggesting the beaches post-date the moraines by some time. New infrared stimulated luminescence (IRSL) dating indicates that beach crests at 5 m above mean sea level were deposited at or shortly before the  $3810 \pm 350$  a and  $4350 \pm 400$  a IRSL ages for the foredune basal sand that overlies the top of the beach crest (further detailed in the supplementary information). Beach crests at <2 m elevation are covered by dune sands and shadow dunes dated to  $1180 \pm 110$  a and  $710 \pm 100$  a respectively. These ages imply that RSL fell from 4-5 m shortly after 4000 yr and has been below 1 m since at least  $\sim 1200$  yr.

Little Jason Lagoon is a coastal basin in inner Cumberland West Bay ( $54^{\circ}11.568'S$   $36^{\circ}35.469'W$ ; detailed in supplementary information). It is near-circular with a narrow entrance and shallow sill at 1 m ( $\pm 0.5$  m) depth. Analysis of a sediment core (Co1305) sampled from within the lagoon has demonstrated that the sediments record a transition from freshwater (lacustrine) conditions to a marine lagoon. The transition from a freshwater to marine environment has been identified on the basis of  $\delta^{13}\text{C}$  of TOC and diatom data with a commensurate increase in measured sulphur at the point

of isolation (Figure 5). Plant remains from 2 cm above the transition yield a radiocarbon age of  $8966 \pm 106$   $^{14}\text{C}$  yr BP (9662-10251 cal yr BP) giving a maximum age for the transition from freshwater to marine conditions in the basin.

Site	Elevation (m asl)	Material dated	$^{14}\text{C}$ age ( $^{14}\text{C}$ yr BP)	Lab code	Age	Comment	Source
King Edward Cove	7.2	Peat on moraine	$9493 \pm 370$	SRR-736	*9677-11832	Maximum age of 7.2 m beach	Clapperton et al. (1978)
Cumberland West Bay	7.2	Peat on raised beach	$3997 \pm 85$	SRR-597	*4148-4645	Minimum age of 7.2 m raised beach	Clapperton et al. (1978)
St Andrews Bay	6	Organic sediment including sea skin and hair	$2369 \pm 40$	SRR-520	*1369-1557	Minimum age for 6 m beach.	Stone (1979)
Little Jason Lagoon	$-1 \pm 0.5$	Plant remains	$8966 \pm 106$		*9662-10251	Timing of freshwater-to-marine transition as RSL rose.	This study
Enten Bay	5.5	Sand		C-L3329	#3980 $\pm$ 340	Minimum age for beach	This study
Enten Bay	5.5	Sand		C-L3330	#4350 $\pm$ 100	Minimum age for beach	This study
Enten Bay	5.7	Sand		C-L3328	#3810 $\pm$ 350	Minimum age for beach	This study
Enten Bay	1.5	Sand		C-L3332	#1180 $\pm$ 110	Minimum age for beach	This study
Enten Bay	1.8	Sand		C-L3331	#710 $\pm$ 100	Minimum age for beach	This study

**Table 1** - Dated relative sea level constraints from South Georgia.

\* (cal yr BP), radiocarbon ages calibrated using CALIB v.7.1 (<http://calib.qub.ac.uk/>) (Stuiver and Reimer, 1993). Reported calibrated ages are the 2-sigma ranges, using the SH13 curve (Hogg et al., 2013). Marine reservoir correction for seal hair taken as 750 yr (Sugden and John, 1973).

# IRSL ages (see Supplementary Info).

The dated RSL data points are compiled in Figure 3 to provide a series of constraints against which the GIA model results can be compared, though the main constraint is the elevation of the ~6-10 m marine limit.

### **Glacial isostatic adjustment modelling**

Modelling of the solid earth response and resulting RSL changes to test the proposed maximum and minimum ice scenarios is done using ALMA (Spada, 2008), which is specifically suitable for GIA regional modelling and high spatial resolutions. ALMA implements the Post Widder formula and computes the Love numbers for a spherical self-gravitating, layered, incompressible Earth model with Maxwell rheology. The viscosity profile is a volume-average of the one adopted in Peltier's (2004) Earth model VM2: lower mantle viscosity  $2.7 \times 10^{21}$  Pa s and upper mantle  $0.5 \times 10^{21}$  Pa s. The lithosphere is elastic with a thickness of 90 km. There is no direct evidence for a low viscosity mantle at this location and this allows us to integrate the ICE-5G (VM2) solutions computed in SELEN (Spada et al., 2012; Spada and Stocchi, 2007) for far-field RSL changes driven by changes in the global ice sheets from their LGM maximum (Figure 6). We do not use ICE-6G model (Argus et al., 2014; Peltier et al., 2015) at this time due to uncertainties surrounding the Antarctic Peninsula component (Purcell et al., 2016), which due to its proximity to South Georgia may have implication for our results. Figure 6 shows that South Georgia experiences relatively minor far-field isostatic effects and the resulting RSL signal from the global model is primarily due to changes in total ocean volume (often termed the eustatic function) (Figure 6B). This global-model RSL curve is added to our local predictions of RSL changes driven by our South Georgia ice-load models. It must be noted that the ICE-5G (VM2) model of Peltier (2004) includes a compressible Earth structure, which may result in  $\sim 0.1$  mm yr<sup>-1</sup> error when computed in our incompressible model.

Our modelling approach seeks to test the two different LGM hypotheses but does not aim to accurately simulate the past ice cap topography due to the limited palaeo-glaciological constraints. For this reason we use a simple 'slab' ice load in order to provide a simple but robust test between extensive (whole continental shelf occupied by ice) and restricted (ice within the island coastline) ice-load models. The extensive shelf model includes 2315 4.74 km diameter discs, with the restricted island-only ice load comprising 202 discs (Figure 7). Using discs has been a long adopted method for gridding ice load (e.g. Tushingham and Peltier, 1991) to minimise overlap and gaps. The model is computed with 15,000 spherical harmonics to allow for the small load diameter (after Bevis et al., 2016). Increasing the number of discs, i.e. decreasing their diameter, increases the computational intensity at no benefit to the results (Bevis et al., 2016). We test different ice-model thicknesses for each maximum and minimum ice scenario in order to understand the sensitivity of our model output to local thickness changes. We develop 8 key scenarios which allow us to test the maximum and minimum load hypotheses, applying ice loads at 1 k yr time-steps in different combinations (Table 2), partly constrained by the geomorphological evidence discussed above. Ice-load histories are given relative to present from 22 to 0 ka, with a constant load from 71 ka to the LGM in order to allow reasonable equilibration of the ice load. In each of the extensive (shelf) or restricted (island) ice models all the discs have the same stepwise ice-load history, and all ice models include a 100 m thick load for the island-only discs at 4-3 ka and 1-0 ka to allow for Neoglacial and recent ice advances (Bentley et al., 2007; Hall, 2009). The model does not allow for underlying topographic variations and therefore the stated values are the uniform ice thickness, not the height of the ice surface with respect to the underlying topography. The limited glaciological evidence for the LGM ice-cap behaviour on South Georgia means that it is not currently feasible to develop spatially variable time-retreating ice-load histories. The model outputs are computed for 12 key locations (Figure 1) including four GPS stations (detailed in Table 3).

Model number	Description	Island (restricted) ice load	Shelf (extensive) ice load
1	Restricted, thin, island only load	22-12 ka: 100 m	-
2	Restricted, thick, island only load	22-12 ka: 1000 m	-
3	Restricted, very thick, island only load	22-21 ka: 3000 m 21-12 ka: 1000 m	-
4	Thick, LGM shelf load, post-LGM small, thin, island only load	22-21 ka: 1000 m 22-12 ka: 100 m	22-21 ka: 1000 m
5	Extensive, thin shelf load, until 15 ka	22-15 ka: 100 m	22-15 ka: 100 m
6	Extensive, thick shelf load, until 18 ka	22-18 ka: 1000 m	22-18 ka: 1000 m
7	Extensive, thick shelf load, until 15 ka	22-15 ka: 1000 m	22-15 ka: 1000 m
8	Extensive, thick shelf load, until 12 ka	22-12 ka: 1000 m	22-12 ka: 1000 m

**Table 2** – South Georgia ice model scenarios used in ALMA

## Results

The results of the ALMA RSL curves for the 12 observer locations on South Georgia, combined with the SELEN modelled ICE-5G RSL curve (Figure 6), are plotted in Figure 8 and compared with the RSL data and marine limit elevations. Fit with the data is assessed visually as the restricted number of available RSL data points and their marine limiting nature means a statistical assessment is not viable. Due to the simplicity of the ice model there is very little spatial variation between the 12 modelled observer locations during the Holocene, so the results are not plotted by separate colours in Figure 8 and are discussed for all the modelled South Georgia sites collectively. All the model outputs predict a rise from a post-LGM lowstand, with the pre-Holocene part of the RSL curves tracking the general RSL rise of the ICE-5G global modelled curve in Figure 6B.

The restricted ice-load models, which only contain ice on the island (models 1-3), as well as model 4 which has 1000 m thick ice on the shelf until 21 ka followed by restricted island-only ice, do not predict a Holocene highstand (Figure 8). The modelled RSL curves are dominated by the global GIA signal with the highest modelled sea level occurring at the present day. The field data provides strong evidence for a period of post-LGM sea level higher than present, which suggests that the restricted ice models do not contain enough local mass to result in a solid earth deformation to fit the geomorphological data, even with the extreme 3000 m thick ice in model 3.

The extensive shelf-edge model with only 100 m of ice (model 5) also does not predict RSL above present (Figure 8). It is only in the load scenarios where the ice thickness is increased to 1000 m in extensive models 6-8 do the outputs predict a period of RSL above present (Figure 8 and S6), demonstrating the importance of local GIA overprinting the far-field derived RSL. In model 6 (18 ka deglaciation) a 0.8 m highstand occurs at 5 ka, and in model 7 (15 ka deglaciation) a 4.2 m highstand occurs at 9 ka. Model 8 (12 ka deglaciation) has a double peaked highstand of 15.9 m at 13 ka, followed by a second of 13.0 m at 9 ka. This is the only model which predicts sea level far above the ca. 6-10 m marine limit implied by the geomorphological sea-level data (Figure 3). The timing of deglaciation in model 8 is also much too late to fit with the evidence of the onset of ice-free conditions at Tønsberg Point (Rosqvist et al., 1999). The output provides a useful maximum load end-member, but we are able to reject this solution. The extensive thick shelf-edge ice loads in models 6 and 7 provide the closest fit with the geomorphological sea-level data, with the higher highstand in model 7 of ca. 4 m, nearest in elevation to the measured marine limit, suggesting this is the optimum scenario. Crucially we find that an extensive thick model with relatively early deglaciation can simulate a highstand of similar timing and magnitude as the field data.

To test the sensitivity of the results with respect to changes in the rheology of the Earth, we combine the deglaciation model 7 with different viscosity profiles (Figure 9), keeping fixed the lithospheric thickness at the ICE-5G(VM2) value of 90 km since we know that this parameter plays a minor role in the GIA response (see Stocchi and Spada, 2009). It should be noted that the results in Figure 9 have mainly a qualitative character, since modifying the VM2 viscosity profile alters the agreement of the ICE-5G (VM2) predictions with the set of global Holocene RSL curves used to calibrate it. As pointed out by Tamisiea (2011), more realistic GIA estimates could be obtained by simultaneously varying the global ice loading history and the rheology, and possibly taking 3D variations in the Earth's properties into account, which is beyond the scope of this work. Due to the relatively small sensitivity of the RSL curves to the site location (Figure 8), we only consider the site of Brown Mountain GPS (Table 3) in

Figure 9. The ranges for the local upper mantle viscosity and the lower mantle viscosity are 0.2 to 0.8 x 10<sup>21</sup> Pa s and 1.0 to 5.0 x 10<sup>21</sup> Pa s, respectively. It is apparent that when the ICE-5G(VM2) upper mantle viscosity is used (0.5 x 10<sup>21</sup> Pa s), a satisfactory fit with the data is obtained for all the lower mantle viscosities considered (the insensitivity to lower mantle viscosity is explained by the relatively small size of the ice load). The misfit increases when the upper mantle viscosity is too low (0.2 x 10<sup>21</sup> Pa s, which implies a fast relaxation) or too high (0.8 x 10<sup>21</sup> Pa s, which enhances the amplitude of the highstand) compared to the VM2 value.

## **Discussion**

### *Testing models of LGM ice extent on South Georgia*

The results of the GIA modelling presented in this paper, when compared to marine limit and RSL data, support the extensive glaciation hypothesis where LGM ice extends to the continental shelf edge (Clapperton et al., 1989; Graham et al., 2008; Sugden and Clapperton, 1977). Even with an extreme ice thickness of 3000 m (which is higher than the elevation of the highest summit, Mount Paget, and does not allow for underlying topography) in the restricted island-only model 3, the GIA outputs cannot produce a highstand to produce a ca. 6-10 m marine limit. Therefore, based upon GIA modelling, it seems unlikely that the restricted glaciation model of Bentley et al. (2007) is valid. The model (7) which provides the best fit with the data, suggests deglaciation of the shelf at ca. 15 ka BP. This is potentially ca. 4 ka later than suggested by the onset of lake sedimentation at Tønsberg Point (Rosqvist et al., 1999). A limitation of our approach is the lack of a spatially variable load and accounting for the underlying topography. It remains possible to fit the RSL data with an extensive ice cap model together with a spatially and temporally variable deglacial history to accommodate early deglaciation at Tønsberg, but this is beyond the scope of this study. This could be revisited when evidence for early deglaciation is found in more than one location.

The results of an extensive LGM ice cap on South Georgia requires the reinterpretation of existing research. As proposed by Graham et al. (2008) this implies that terrestrial and fjord moraines mapped by Bentley et al. (2007) and Hodgson et al. (2014a) are in fact either retreat, stillstand or readvance margins of a post-LGM ice cap, formed subsequently to the maximum extension of the ice onto the continental shelf. The moraines mapped by Graham et al. (2008) at the shelf edge are therefore most likely to be LGM in age and a programme of offshore dating could establish this. Both Sugden and Clapperton (1977) and Hodgson et al. (2014a) suggest that the offshore evidence of glacial erosion may be from a previous Pleistocene extensive glaciation. However, we are able to produce modelled elevations of RSL which fit with the geomorphological data based upon the simplest explanation of a large LGM ice cap, avoiding the complication of multiple phases of GIA through multiple glacial-interglacial cycles.

Our results also have implications for the long-term evolution of the island. Given the difficulty of producing substantive highstands in the GIA models, even with a very substantial extensive ice cap it seems unlikely that the rock platforms could have been formed at their current elevations (20-50m) due to GIA alone. This is particularly apparent when their size is taken into account as they would potentially have needed substantial periods of time to be eroded. It seems more likely that they may have formed during one or more previous interglacial highstands, implying long-term uplift of the island. We also cannot rule out that the platforms are entirely pre-glacial. Long-term uplift is consistent with thermochronological data that suggest the island may have seen significant exhumation since 10 Ma (Carter et al., 2014). Given that the platforms have survived at least one glaciation, possibly several, we suggest that the LGM ice cap on South Georgia was not particularly efficient at eroding pre-existing deposits (e.g. preserved beach material up to 52 m asl) or the higher rock platforms. The non-erosion of more extensive raised beaches and enclosed marine fauna on Prince Karls Forland on western Svalbard (Evans and Rea, 2005; Landvik et al., 2005; Mangerud et al., 1996; Miller et al., 1989) and on eastern Baffin Island (Davis et al., 2006), even though they have been

overrun by glacier ice, constitute examples of similarly ineffective glacial erosion of pre-existing deposits at low elevations around the margins of an ice sheet-covered archipelago similar to South Georgia. Whether, like the Svalbard and Baffin Island examples, the survival of raised marine features was related to cold-based ice sheet marginal conditions or just localized ineffective erosion cannot be determined at this stage.

#### *Ongoing land-level change on South Georgia*

The available RSL data that constrains our GIA models is limited and precludes the development of a spatially variable ice load model. Aside from collecting further geomorphological evidence of RSL change, there may be potential to further constrain the spatial and temporal ice history of future models using instrumental data based upon the spatial pattern of modern rates of land-level change. The first global navigation satellite system (GNSS) station in South Georgia was installed on Brown Mountain (station: KEPA), King Edward Point in February 2013 with the aim of providing a reference point for the King Edward Point tide gauge and constrain tectonic motion of South Georgia (Teferle, *pers. comm.*). Three additional stations were installed in October 2014 at northern (SOG2), southern (SOG1) and eastern (SOG3) locations in South Georgia (Dalziel, *pers. comm.*). The short duration of the records means they are not yet suitable to use as constraints in this study, but a network of GPS locations providing detailed information as to the spatial pattern of present day rates of land-level change may help resolve model outputs further and allow for more complex ice load histories to be tested in the absence of geomorphological constraints. In the meantime, using the ALMA outputs of the local ice cap in Model 7 (Figure 8) and outputs from SELEN (Figure 6), we are able to provide estimates of present rates of vertical uplift at the four GPS sites as explained by the local and global modelled GIA (Table 3). Differences between these estimates and measured vertical rates may be ascribable to tectonics, local GIA or the selected Earth model (Figure 9).

<b>Model observer location Longitude and Latitude (deg)</b>	<b>Nearest GNSS station</b>	<b>Local ice history (ALMA) modelled uplift (mm yr<sup>-1</sup>)</b>	<b>Global ice history (SELEN) modelled uplift (mm yr<sup>-1</sup>)</b>	<b>Total modelled GIA uplift (mm yr<sup>-1</sup>)</b>
Brown Mountain -36.50 -54.30	KEPA	0.52	0.45	0.97
Annenkov Island -37.04 -54.49	SOG3	0.44	0.44	0.88
Northwest South Georgia -38.05 -54.00	SOG2	0.37	0.46	0.83
Southeast South Georgia -36.04 -54.87	SOG1	0.43	0.42	0.85

**Table 3** – Modelled rate of vertical displacement due to post-LGM glacial isostatic adjustment as computed by the models detailed in this paper at the four GPS locations on South Georgia. Locations from N. Teferle, (*pers. comm.*) and Dalziel, (*pers. comm.*). More information is available at <https://www.unavco.org/data/gps-gnss/gps-gnss.html>

#### *Wider implications of an extensive LGM ice cap on South Georgia*

The suggestion of an extensive thick ice cap on South Georgia has implications for other sub-Antarctic islands, on which limited geomorphological evidence is recorded, but where there exists similar debate about the extent of Quaternary glaciation(s) (Hodgson et al., 2014b; Sugden and Clapperton, 1977). If a large LGM ice cap existed in South Georgia then there is potential for the same to have occurred on other sub-Antarctic islands within a similar climatic context e.g. Kerguelen, and also fits with other models of extensive LGM ice proposed for Heard, Bouvet and the South Orkney Islands (Hodgson et al., 2014b). The presence of an extensive LGM ice cap that reached the continental shelf edge around South Georgia suggests affinity with West Antarctica and the Antarctica Peninsula, which also experienced the most extensive glaciation at the LGM, rather than with Patagonia where the greatest glacial extents were earlier in the Quaternary (Darvill et al., 2015). Our model results suggests that deglaciation on South Georgia occurred ca. 15 ka, which fits with geomorphological data from the east Antarctic Peninsula where initial retreat was underway by ~18-17.5 ka (Bentley et al., 2014), as

well as dates of the onset of peat formation and lake sedimentation at other sub-Antarctic islands, including Kerguelen, Auckland and Campbell, around this time (Hodgson et al., 2014b).

Our conclusion of an extensive ice cap extending to the shelf edge would imply that if there were any biological refugia around South Georgia, they must have been relatively localised and restricted to the outermost shelf and any potential nunataks. Our model is not spatially variable and so we are unable to determine the locations of these refugia using current datasets. Our fits with a recent assessment of the seabed biodiversity around South Georgia which concludes that most of the shelf is still undergoing recolonization following glacial retreat (Barnes et al., 2016).

The approach presented here, to use GIA modelling and associated RSL data to differentiate between opposing models of ice extent, may also be applied in other locations where similar debates exist, e.g. Iceland (Brader, 2015). The order-of-magnitude difference of the modelled RSL changes as a result of the maximum versus minimum ice extent models, means this approach is able to provide a first order test of the hypotheses without the need for detailed glacial histories. This is particularly valuable where offshore data is limited or lacks a chronology. However, not all current GIA models are designed to work at the sufficiently high enough number of spherical harmonics required to resolve differences between relatively small ice loads. Thus, a bespoke solution, such as used here with the flexible code in SELEN and ALMA (Spada, 2008; Spada et al., 2012; Spada and Stocchi, 2007), may be required.

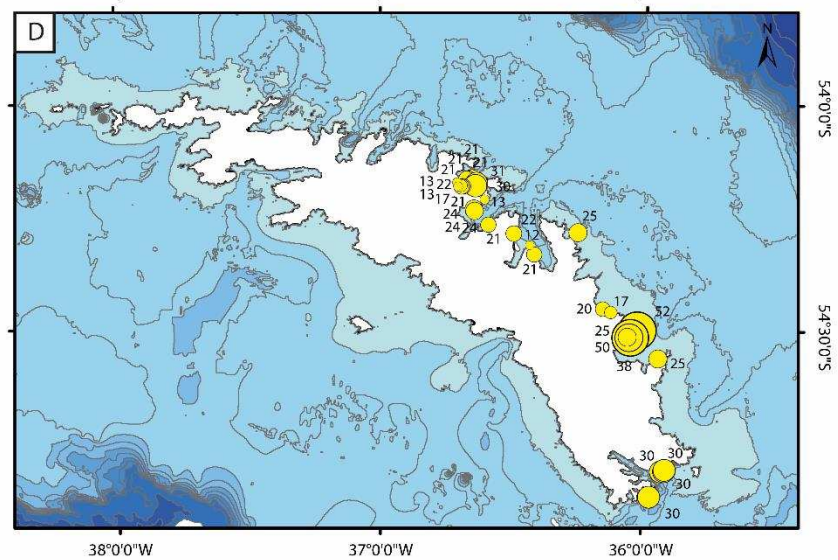
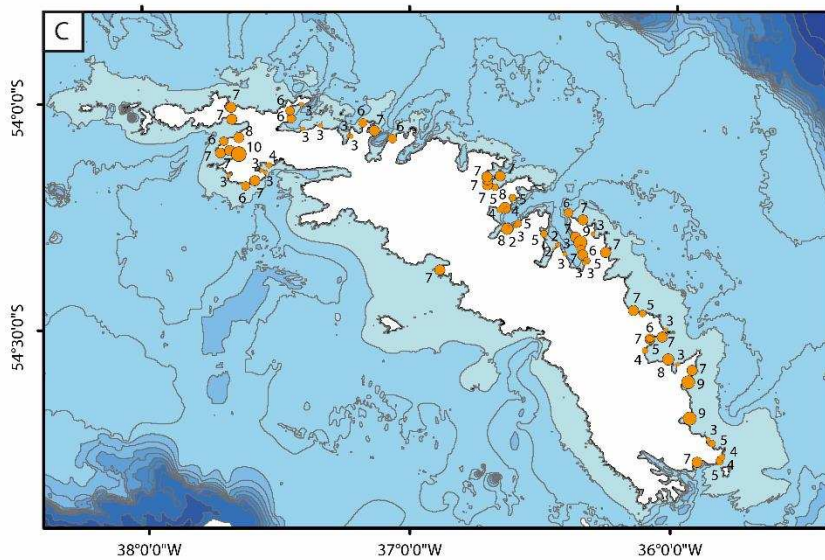
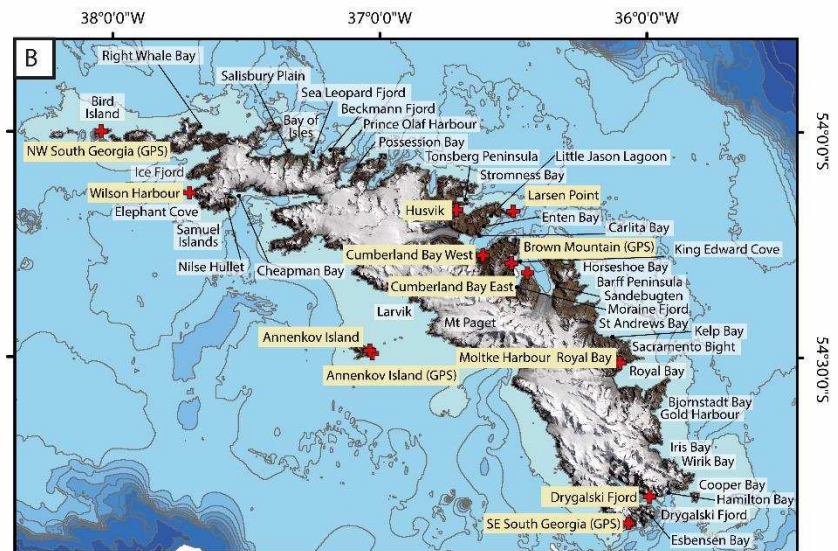
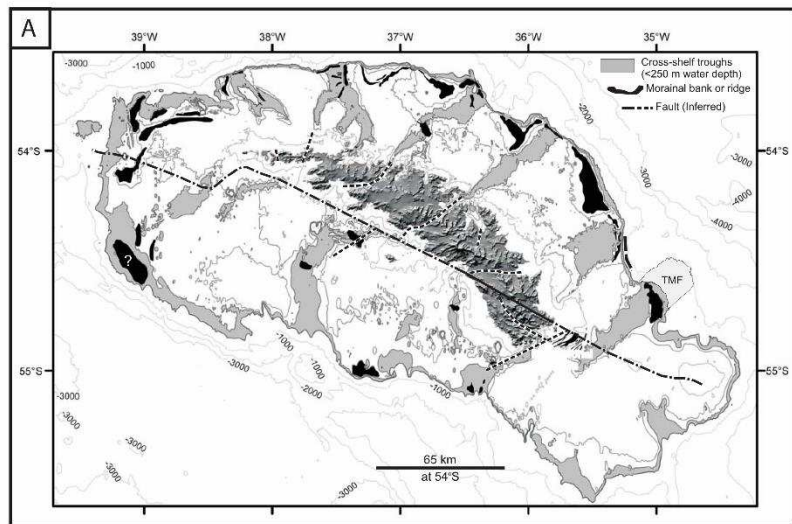
## **Conclusions**

We conclude from our GIA modelling and constrained by a newly-compiled RSL dataset, that the LGM glaciation of South Georgia was extensive and extended to the shelf edge at a time when the island was covered by thick (>1000 m) ice. Deglaciation occurred relatively early, indeed our best fit model suggests substantial deglaciation by ca. 15 ka BP, although independent data suggests this may have been as early as 18 ka in places. Further work should seek to define the geometry of the South Georgia

ice cap and the date and timing of deglaciation in order to allow the development of a more sophisticated and spatially-variable ice model. This will also require the collection of additional sea level index points to constrain the modelled outputs, and comparison of GPS-derived uplift rates to our GIA modelled present day rates of change.

## **Acknowledgements**

We thank the Royal Scottish Geographical Society (RSGS), Carnegie Trust for the Universities of Scotland, and National Geographic for fieldwork support and to the members of the RSGS *Scotia* expedition for field assistance. We are also grateful to the Government of South Georgia and the South Sandwich Islands for permits and assistance in our work. This paper has benefited from discussions with Alastair Graham (who also provided Figure 1A), Dominic Hodgson and Pippa Whitehouse, members of PALSEA2 (an INQUA International Focus Group and a PAGES working group) and the Quaternary Research Association Sea Level and Coastal Change (SLaCC) working group. G.S. is funded by Programma Nazionale di Ricerche in Antartide (PNRA) 2013/B2.06 (CUP D32I14000230005). Reviewers by Alex Simms and an anonymous reviewer improved this manuscript.



0 5 10 20 40 Kilometers

**Figure 1:** Location Maps of South Georgia. (a) Summary map of bathymetry and geomorphology of South Georgia and its surrounding continental shelf (from Graham et al., 2008). Fault (dot-dash line) inferred from onshore expression of strike-slip fault (solid line) in the south east of the island. TMF, trough mouth fan. (b) Location Map of South Georgia. All place names are taken from map: South Georgia 1:200k, British Antarctic Survey Misc Sheet 12A and 12B. Red crosses mark locations of model predictions, including GPS sites in Table 3). (c) Raised beaches around South Georgia. Dots are scaled according to size and the elevation (m asl) of the *highest* beach or marine limit is shown beside symbol. (d) Rock platforms around South Georgia. Dots are scaled according to size and the elevation (m asl) of the rock platform is shown beside symbol.

## Raised beaches



## Rock platforms



**Figure 2:** Photographs of examples of the coastal geomorphology of South Georgia. A) Upper (7 m asl) and lower (3 m asl) shorelines at Antarctic Bay, B) Raised beaches at the snout of the Nordensjold

in Cumberland Bay, C) Raised beaches at Moraine Fjord, and D) Raised beaches at Sandebugten, Barff Peninsula. E) Rock platforms at Stromness Bay, F) Rock platform at Tønsberg Peninsula, G) Rock platforms at Carlita Bay and H) Rock platform at Tønsberg Peninsula.

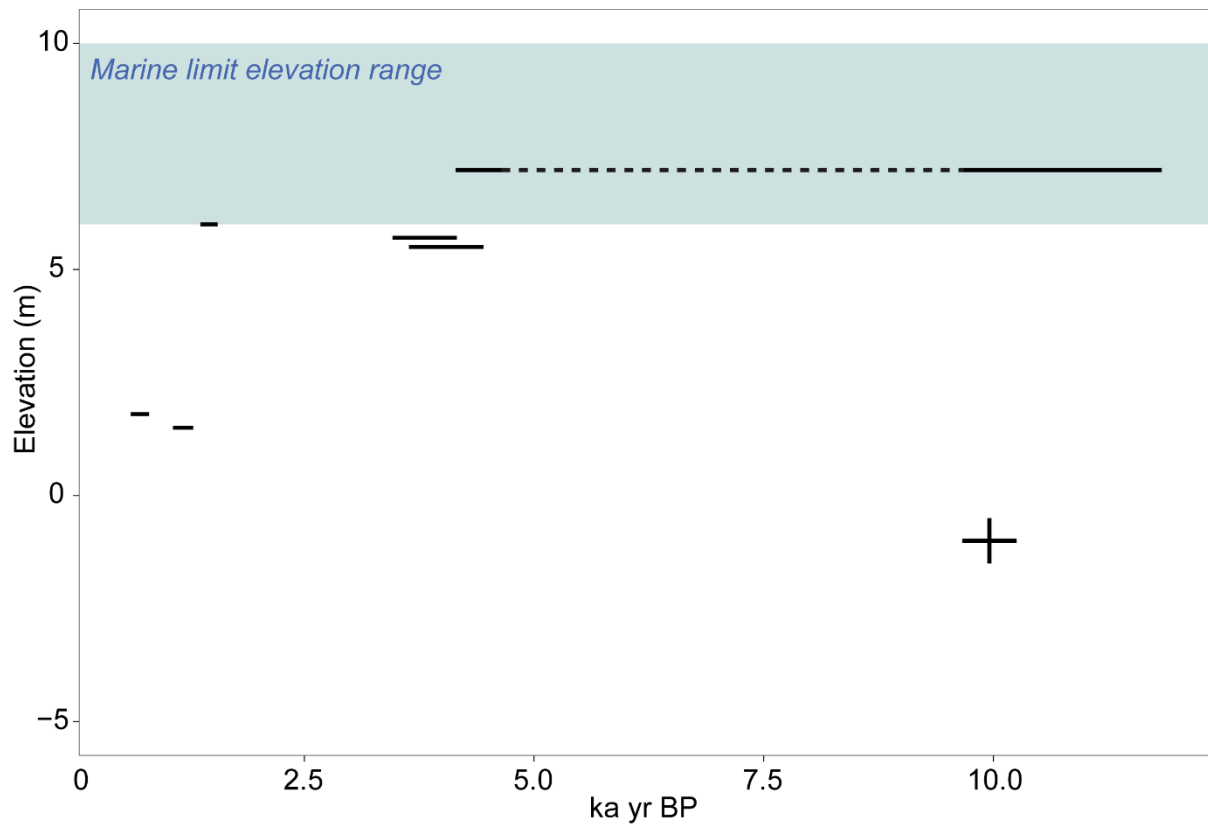


**Figure 3:** Relative sea-level data for South Georgia (from Table 1). Blue band gives 6-10 m typical range of highest raised beaches mapped on the island (references in text and supplementary information Tables S1 and S2). Dotted line joins the maximum and minimum ages of the formation of the raised beach at St Andrews Bay.

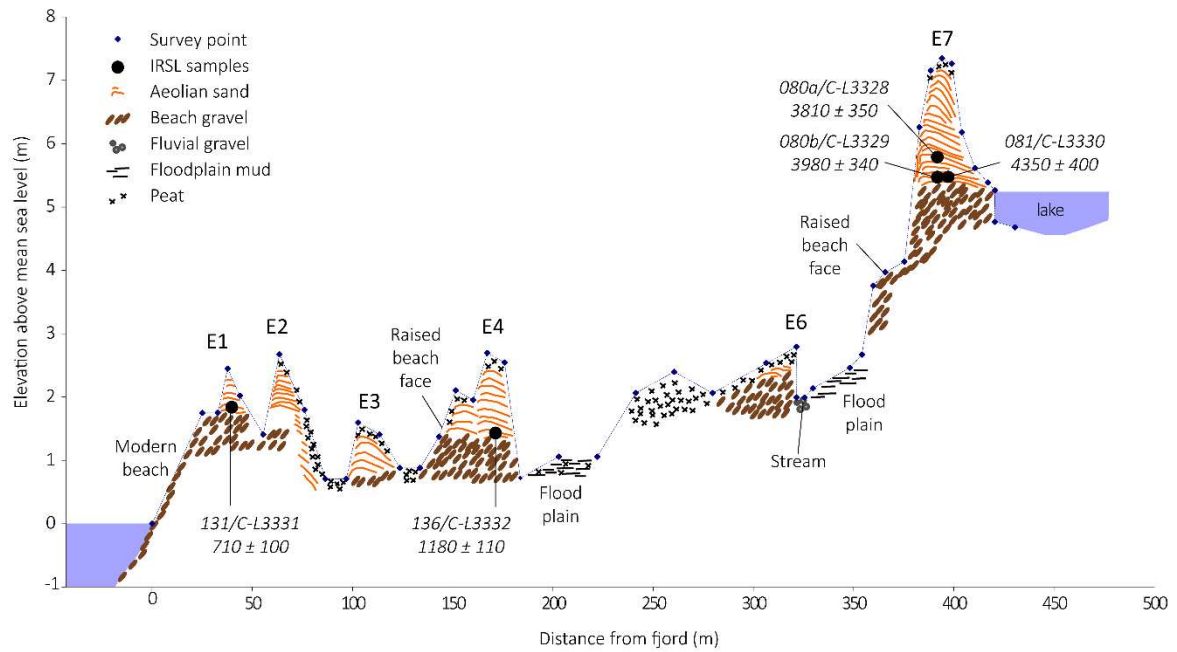


**Figure 4:** Topographic and geologic cross section through the centre of Enten Valley from Cumberland Fjord (left) ~400 m west to a small beach-dammed lake (right). Luminescence ages are shown with field/lab codes (detailed in Table S3), while major beach ridges are labelled E1-7, though E5 is not well expressed on this transect and not marked.

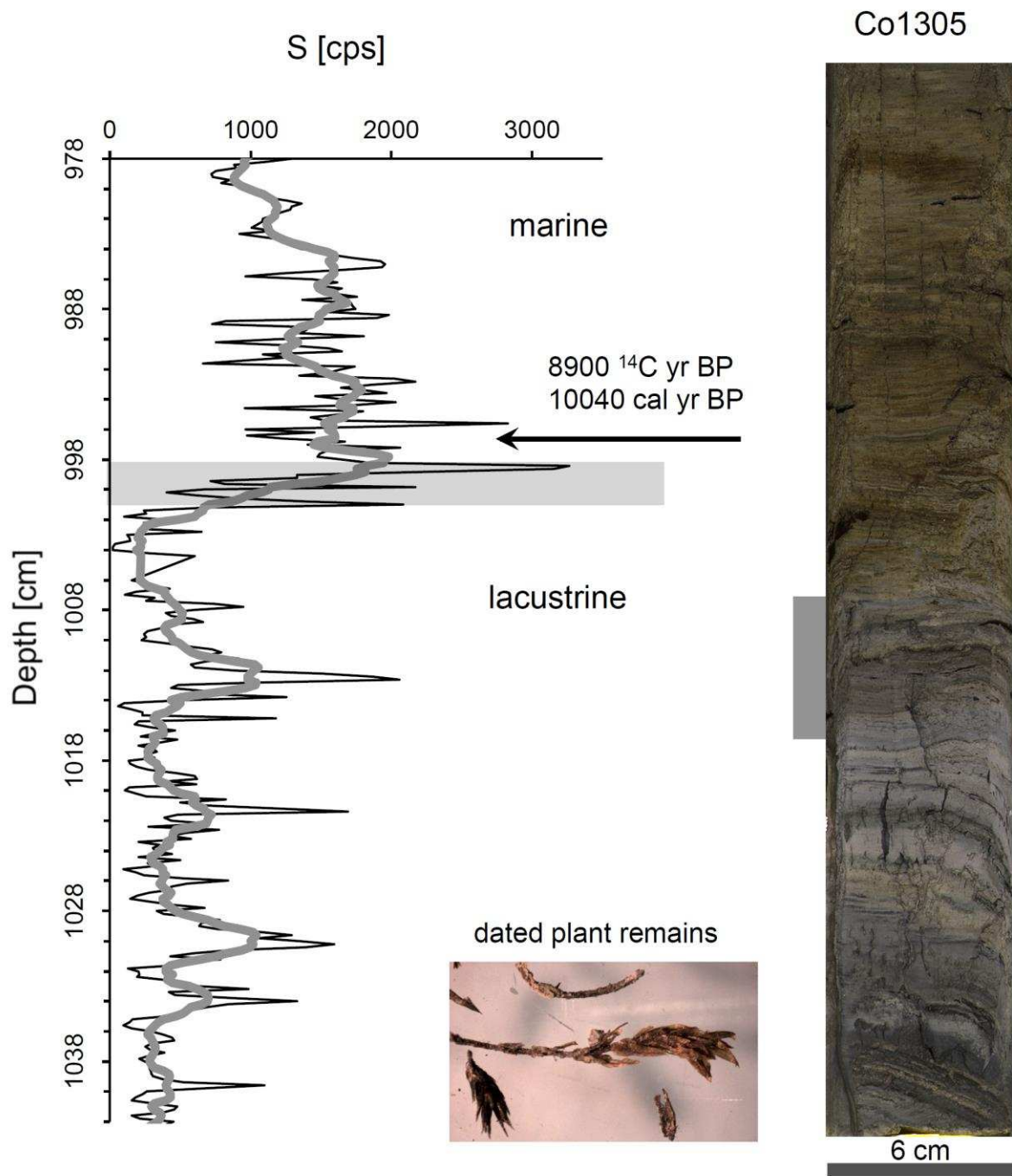


**Figure 5:** Sulphur counts (black line 2mm and grey line 2cm running average) obtained with an XRF core scanner for core Co1305 (1042 to 978 cm depth) from Little Jason Lagoon. Line scan image of the core section containing the lacustrine/marine transition. Grey bar indicates the position of increase in sulphur. Arrow indicates position of the radiocarbon dated plant remains.

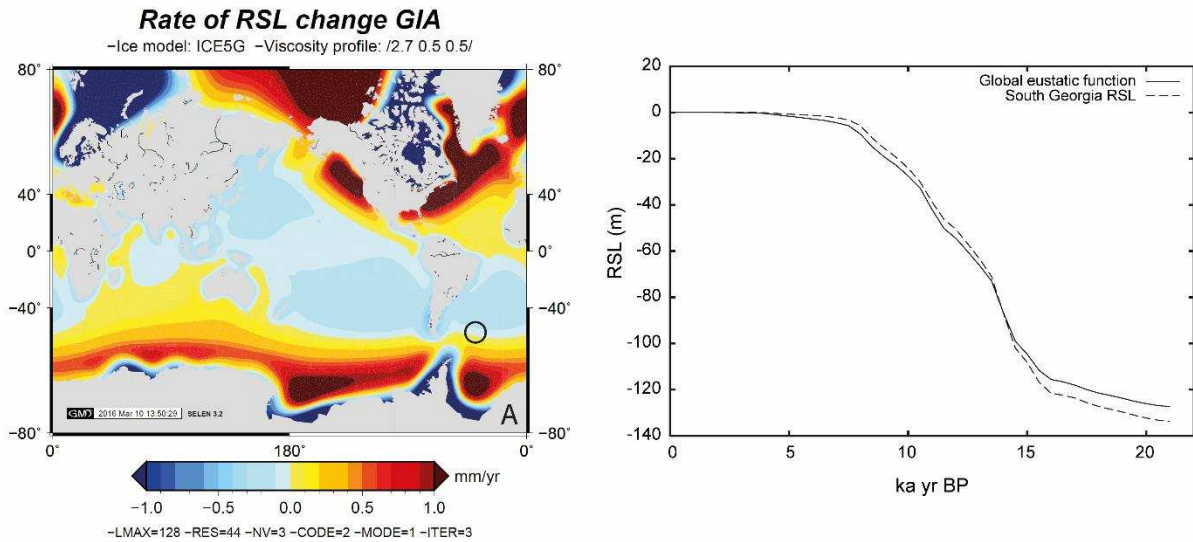


**Figure 6:** A: Map of present day rates of relative sea-level change modelled in SELEN using ICE-5G and a VM2 average viscosity (details on Figure). B: Relative sea-level changes due to global GIA at South Georgia (dotted line) are similar to the global (eustatic) changes in ice volume in ICE-5G (solid line).

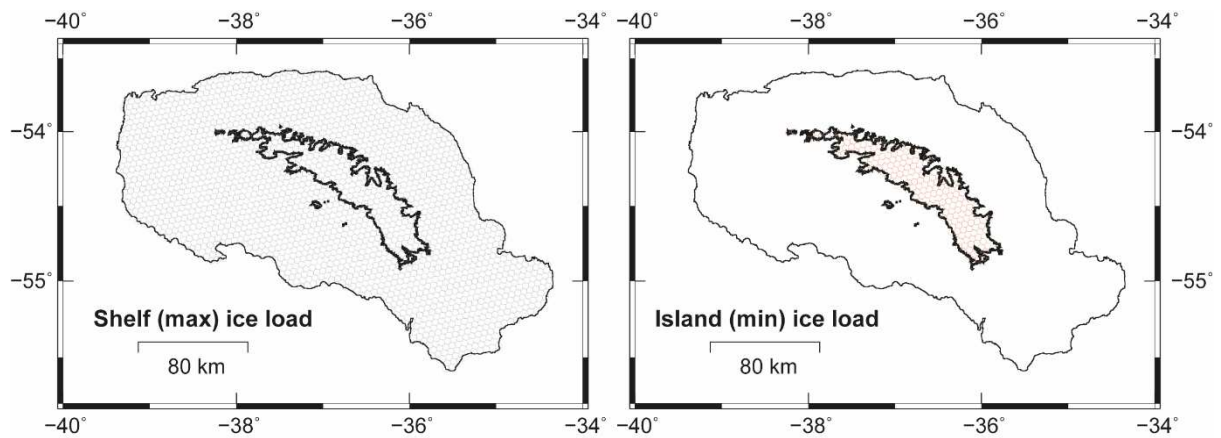


**Figure 7:** Disc ice loads extents in ALMA for the extensive shelf (maximum) and restricted (minimum) island-only models in Table 2. Colours match those in the ice thickness histories in Figure 8.

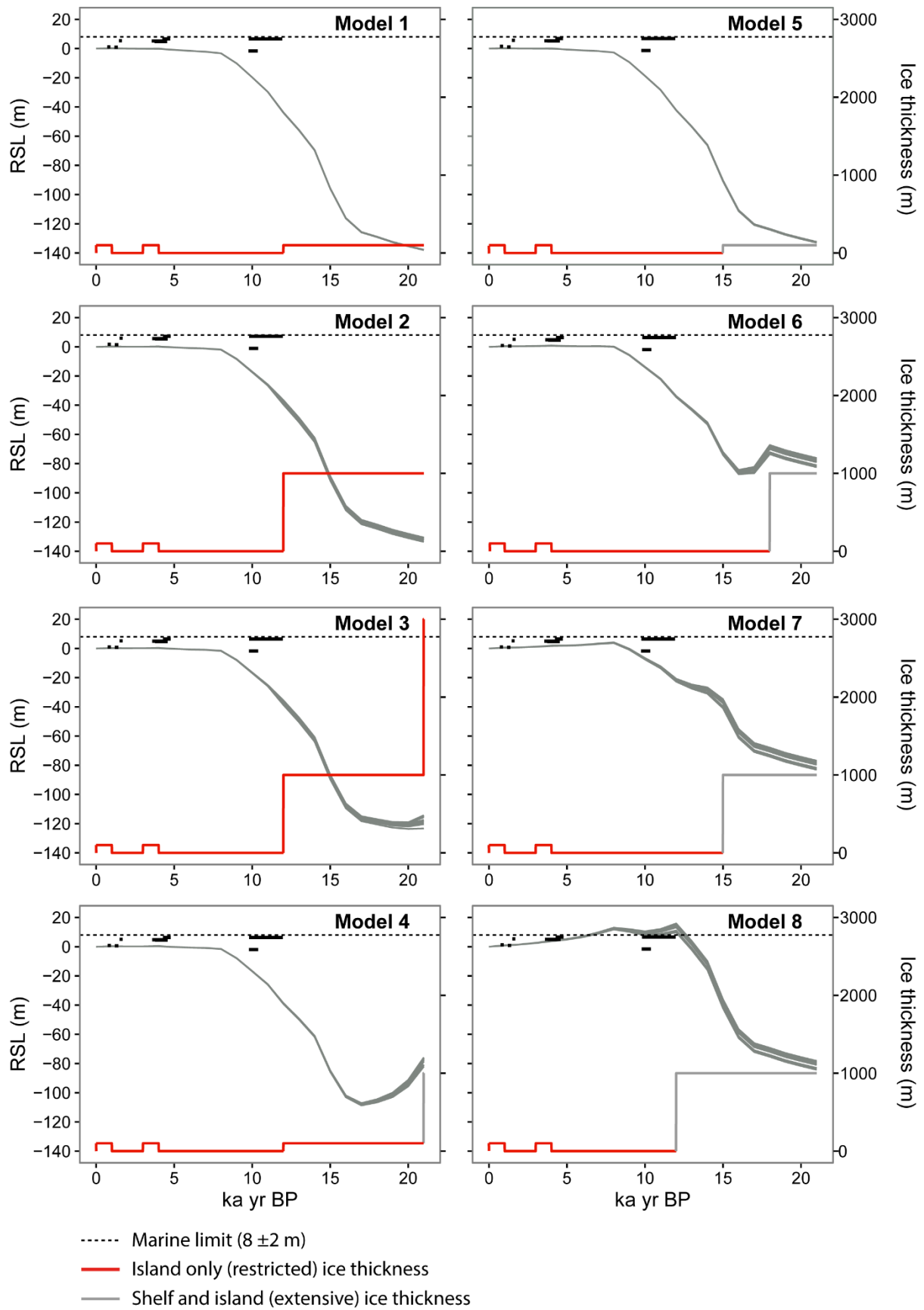


**Figure 8:** Modelled relative sea-level changes using the 8 ice models detailed in Table 2 plotted against data from Figure 3 (note blue band of marine limit in Figure 3 shown as dotted line here for simplicity). Relative sea-level curves are a combination of the ALMA modelled outputs in response to the ice thickness changes plotted in each graph (colours correspond to the ice models in Figure 7) combined with the South Georgia SELEN global model relative sea level in Figure 6B. Note, output for all the 12 observer locations are plotted in a single colour as they are so similar it is not possible to visually separate them.

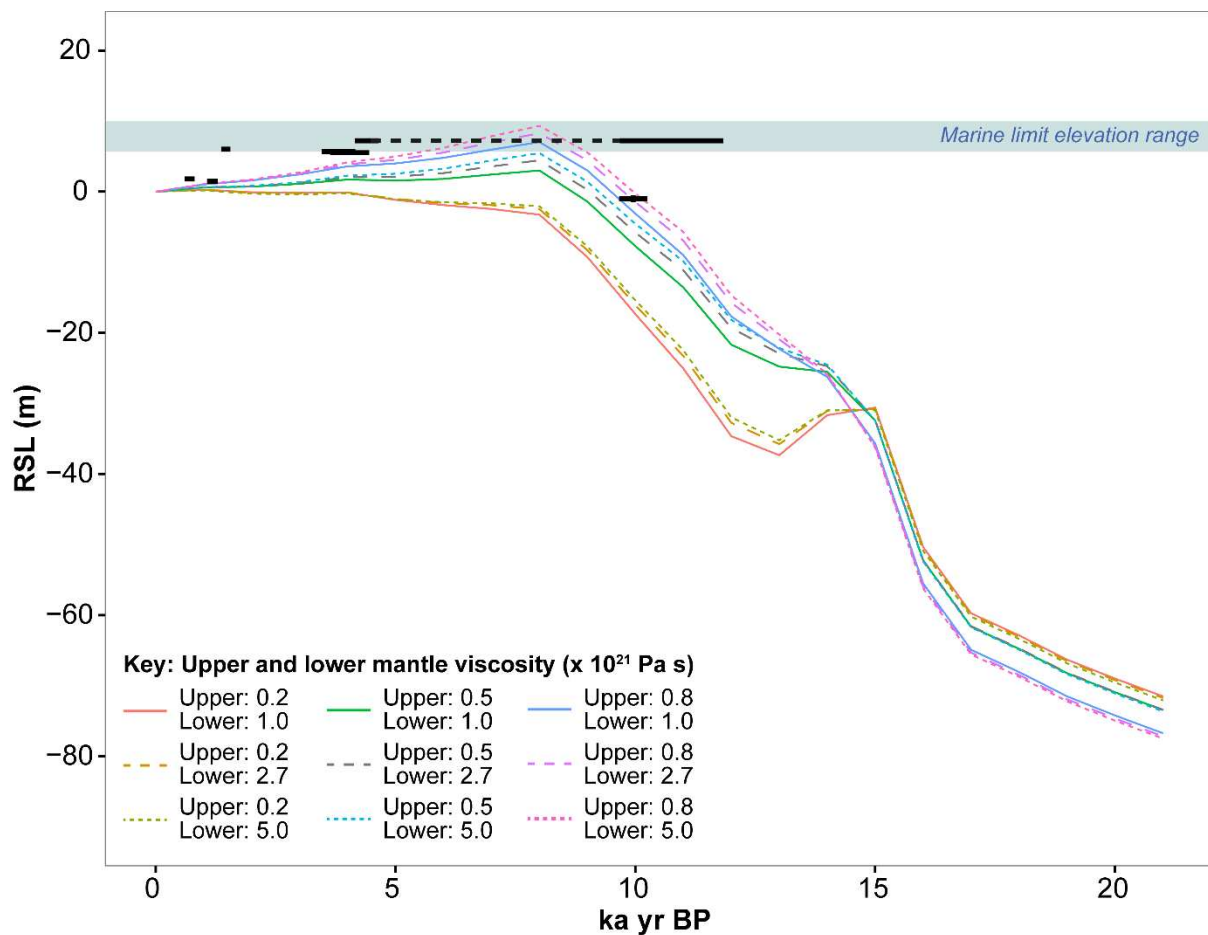


**Figure 9:** Modelled relative sea-level changes at the Brown Mountain GPS station using ice model 7 (detailed in Table 2) and a range of upper and lower mantle viscosities ( $\times 10^{21}$  Pa s) plotted against relative sea level data from Figure 3. Earth model used in outputs in Figure 8 shown by grey dotted line.

## References

- Adie, R.J., 1964. Sea level changes in the Scotia Arc and Graham Land, in: Adie, R.J. (Ed.), *Antarctic Geology*. North-Holland Publishing Company, Amsterdam, pp. 27-32.
- Argus, D.F., Peltier, W.R., Drummond, R., Moore, A.W., 2014. The Antarctica component of postglacial rebound model ICE-6G\_C (VM5a) based on GPS positioning, exposure age dating of ice thicknesses, and relative sea level histories. *Geophysical Journal International* 198, 537-563.
- Barnes, D.K.A., Hodgson, D.A., Convey, P., Allen, C.S., Clarke, A., 2006. Incursion and excursion of Antarctic biota: past, present and future. *Global Ecology and Biogeography* 15, 121-142.
- Barnes, D.K.A., Sands, C.J., Hogg, O.T., Robinson, B.J.O., Downey, R.V., Smith, J.A., 2016. Biodiversity signature of the Last Glacial Maximum at South Georgia, Southern Ocean. *Journal of Biogeography*, n/a-n/a.
- Bentley, M.J., Evans, D.J.A., Fogwill, C.J., Hansom, J.D., Sugden, D.E., Kubik, P.W., 2007. Glacial geomorphology and chronology of deglaciation, South Georgia, sub-Antarctic. *Quaternary Science Reviews* 26, 644-677.
- Bentley, M.J., Ó Cofaigh, C., Anderson, J.B., Conway, H., Davies, B., Graham, A.G.C., Hillenbrand, C.-D., Hodgson, D.A., Jamieson, S.S.R., Larter, R.D., Mackintosh, A., Smith, J.A., Verleyen, E., Ackert, R.P., Bart, P.J., Berg, S., Brunstein, D., Canals, M., Colhoun, E.A., Crosta, X., Dickens, W.A., Domack, E., Dowdeswell, J.A., Dunbar, R., Ehrmann, W., Evans, J., Favier, V., Fink, D., Fogwill, C.J., Glasser, N.F., Gohl, K., Gollledge, N.R., Goodwin, I., Gore, D.B., Greenwood, S.L., Hall, B.L., Hall, K., Hedding, D.W., Hein, A.S., Hocking, E.P., Jakobsson, M., Johnson, J.S., Jomelli, V., Jones, R.S., Klages, J.P., Kristoffersen, Y., Kuhn, G., Leventer, A., Licht, K., Lilly, K., Lindow, J., Livingstone, S.J., Massé, G., McGlone, M.S., McKay, R.M., Melles, M., Miura, H., Mulvaney, R., Nel, W., Nitsche, F.O., O'Brien, P.E., Post, A.L., Roberts, S.J., Saunders, K.M., Selkirk, P.M., Simms, A.R., Spiegel, C., Stollendorf, T.D., Sugden, D.E., van der Putten, N., van Ommen, T., Verfaillie, D., Vyverman, W., Wagner, B., White, D.A., Witus, A.E., Zwart, D., 2014. A community-based geological reconstruction of Antarctic Ice Sheet deglaciation since the Last Glacial Maximum. *Quaternary Science Reviews* 100, 1-9.
- Bevis, M., Melini, D., Spada, G., 2016. On computing the geoelectric response to a disk load. *Geophysical Journal International* 205, 1804-1812.
- Brader, M.D., 2015. Postglacial relative sea-level changes and the deglaciation of northwest Iceland, Department of Geography. Durham University.
- Carter, A., Curtis, M., Schwanethal, J., 2014. Cenozoic tectonic history of the South Georgia microcontinent and potential as a barrier to Pacific-Atlantic through flow. *Geology* 42, 299-302.
- Clapperton, C.M., 1971. *Geomorphology of the Stromness Bay-Cumberland Bay area, South Georgia*, British Antarctic Survey Scientific reports No. 70. Natural Environment Research Council.
- Clapperton, C.M., Sugden, D.E., Birnie, J., Wilson, M.J., 1989. Late-glacial and Holocene glacier fluctuations and environmental change on South Georgia, Southern Ocean. *Quaternary Research* 31, 210-228.
- Clapperton, C.M., Sugden, D.E., Birnie, R.V., Hansom, J.D., Thom, G., 1978. Glacier fluctuations in South Georgia and comparison with other island groups in the Scotia Sea, in: Bakker, V.Z. (Ed.), *Antarctic Glacial History and World Palaeoenvironments*, Balkema Rotterdam.
- Cook, A.J., Poncet, S., Cooper, A.P.R., Herbert, D.J., Christie, D., 2010. Glacier retreat on South Georgia and implications for the spread of rats. *Antarctic Science* 22, 255-263.
- Darvill, C.M., Bentley, M.J., Stokes, C.R., Hein, A.S., Rodés, Á., 2015. Extensive MIS 3 glaciation in southernmost Patagonia revealed by cosmogenic nuclide dating of outwash sediments. *Earth and Planetary Science Letters* 429, 157-169.
- Davis, P.T., Briner, J.P., Coulthard, R.D., Finkel, R.W., Miller, G.H., 2006. Preservation of Arctic landscapes overridden by cold-based ice sheets. *Quaternary Research* 65, 156-163.
- Evans, D.J.A., Rea, B.R., 2005. Late Weichselian deglaciation and sea level history of St Jonsfjorden, Spitsbergen: A contribution to ice sheet reconstruction. *Scottish Geographical Journal* 121, 175-201.
- Gordon, J.E., Hansom, J.D., 1986. Beach Forms and Changes Associated with Retreating Glacier Ice, South Georgia. *Geografiska Annaler. Series A, Physical Geography* 68, 15-24.

Gordon, J.E., Haynes, V.M., Hubbard, A., 2008. Recent glacier changes and climate trends on South Georgia. *Global and Planetary Change* 60, 72-84.

Gordon, J.E., Timmis, R.J., 1992. Glacier fluctuations on South Georgia during the 1970s and early 1980s. *Antarctic Science* 4, 215-226.

Graham, A.G.C., Fretwell, P.T., Larter, R.D., Hodgson, D.A., Wilson, C.K., Tate, A.J., Morris, P., 2008. A new bathymetric compilation highlighting extensive paleo-ice sheet drainage on the continental shelf, South Georgia, sub-Antarctica. *Geochemistry, Geophysics, Geosystems* 9, n/a-n/a.

Gregory, J.W., 1915. The physiography of South Georgia as shown by Mr Ferguson's photographs, in: Ferguson, D. (Ed.), *Geological Observations in South Georgia*, Transactions of the Royal Society of Edinburgh, pp. 814-816.

Hall, B.L., 2009. Holocene glacial history of Antarctica and the sub-Antarctic islands. *Quaternary Science Reviews* 28, 2213-2230.

Hansom, J.D., 1979. Beach Form and Process Variation in South Georgia, a sub-Antarctic Island. University of Aberdeen, Unpublished PhD thesis.

Hodgson, D.A., Graham, A.G.C., Griffiths, H.J., Roberts, S.J., Cofaigh, C.Ó., Bentley, M.J., Evans, D.J.A., 2014a. Glacial history of sub-Antarctic South Georgia based on the submarine geomorphology of its fjords. *Quaternary Science Reviews* 89, 129-147.

Hodgson, D.A., Graham, A.G.C., Roberts, S.J., Bentley, M.J., Cofaigh, C.Ó., Verleyen, E., Vyverman, W., Jomelli, V., Favier, V., Brunstein, D., Verfaillie, D., Colhoun, E.A., Saunders, K.M., Selkirk, P.M., Mackintosh, A., Hedding, D.W., Nel, W., Hall, K., McGlone, M.S., Van der Putten, N., Dickens, W.A., Smith, J.A., 2014b. Terrestrial and submarine evidence for the extent and timing of the Last Glacial Maximum and the onset of deglaciation on the maritime-Antarctic and sub-Antarctic islands. *Quaternary Science Reviews* 100, 137-158.

Hogg, A.G., Hua, Q., Blackwell, P.G., Niu, M., Buck, C.E., Guilderson, T.P., Heaton, T.J., Palmer, J.G., Reimer, P.J., Reimer, R.W., Turney, C.S.M., Zimmerman, S.R.H., 2013. SHCal13 Southern Hemisphere Calibration, 0–50,000 Years cal BP.

Hogg, O.T., Barnes, D.K., Griffiths, H.J., 2011. Highly diverse, poorly studied and uniquely threatened by climate change: an assessment of marine biodiversity on South Georgia's continental shelf. *Plos One* 6, e19795.

Kelsey, H.M., 2015. Geomorphological indicators of past sea levels, *Handbook of Sea-Level Research*. John Wiley & Sons, Ltd, pp. 66-82.

Landvik, J.Y., Ingolfsson, O., Mienert, J., Lehman, S.J., Solheim, A., Elverhoi, A., Ottesen, D., 2005. Rethinking Late Weichselian ice-sheet dynamics in coastal NW Svalbard. *Boreas* 34, 7-24.

Mangerud, J., Jansen, E., Landvik, J.Y., 1996. Late Cenozoic history of the Scandinavian and Barents Sea ice sheets. *Global and Planetary Change* 12, 11-26.

Miller, G.H., Sejrup, H.P., Lehman, S.J., Forman, S.L., 1989. Glacial history and marine environmental change during the last interglacial-glacial cycle, western Spitsbergen, Svalbard. *Boreas* 18, 273-296.

Peltier, W.R., 2004. Global glacial isostasy and the surface of the ice-age earth: The ICE-5G (VM2) model and GRACE. *Annual Review of Earth and Planetary Sciences* 32, 111-149.

Peltier, W.R., Argus, D.F., Drummond, R., 2015. Space geodesy constrains ice age terminal deglaciation: The global ICE-6G\_C (VM5a) model. *Journal of Geophysical Research: Solid Earth* 120, 450-487.

Purcell, A., Tregoning, P., Dehecq, A., 2016. An assessment of the ICE6G\_C(VM5a) glacial isostatic adjustment model. *Journal of Geophysical Research: Solid Earth* 121, 3939-3950.

Rosqvist, G.C., Rietti-Shati, M., Shemesh, A., 1999. Late glacial to middle Holocene climatic record of lacustrine biogenic silica oxygen isotopes from a Southern Ocean island. *Geology* 27, 967-970.

Smith, J., 1960. Glacier problems in South Georgia. *Journal of Glaciology* 705-714.

Spada, G., 2008. ALMA, a Fortran program for computing the viscoelastic Love numbers of a spherically symmetric planet. *Computers & Geosciences* 34, 667-687.

Spada, G., Melini, D., Galassi, G., Colleoni, F., 2012. Modeling sea level changes and geodetic variations by glacial isostasy: the improved SELEN code. arXiv preprint arXiv:1212.5061.

- Spada, G., Stocchi, P., 2007. SELEN: A Fortran 90 program for solving the "sea-level equation". *Computers & Geosciences* 33, 538-562.
- Stocchi, P., Spada, G., 2009. Influence of glacial isostatic adjustment upon current sea level variations in the Mediterranean. *Tectonophysics* 474, 56-68.
- Stone, P., 1974. Physiography of the North-east coast of South Georgia, *British Antarctic Survey Bulletin*, pp. 17-36.
- Stone, P., 1976. Raised marine and glacial features of the Cooper Bay-Wirik Bay area, South Georgia, *British Antarctic Survey Bulletin*. 44, 47-56.
- Stone, P., 1979. Raised Marine features on the south side of Royal Bay, South Georgia, *British Antarctic Survey Bulletin*, pp. 137-141.
- Stuiver, M., Reimer, P.J., 1993. Extended 14C database and revised CALIB 3.0 radiocarbon calibration program. *Radiocarbon* 35, 215-230.
- Sugden, D.E., Clapperton, C.M., 1977. The maximum ice extent on island groups in the Scotia sea, Antarctica. *Quaternary Research* 7, 268-282.
- Sugden, D.T., John, B.S., 1973. The ages of glacier fluctuations in the South Shetland Islands, Antarctica, Palaeoecology of Africa, the Surrounding Islands and Antarctica. Balkema, Cape Town, pp. 141-159.
- Tamisiea, M.E., 2011. Ongoing glacial isostatic contributions to observations of sea level change. *Geophysical Journal International* 186, 1036-1044.
- Thatje, S., Hillenbrand, C.-D., Mackensen, A., Larter, R., 2008. Life Hung by a Thread: Endurance of Antarctic Fauna in Glacial Periods. *Ecology* 89, 682-692.
- Tushingham, A.M., Peltier, W.R., 1991. Ice-3G: a new global model of late Pleistocene de-glaciation based upon geophysical predictions of post-glacial relative sea level change. *Journal of Geophysical Research* 96, 4497-4523.

## Testing models of ice cap extent, South Georgia, sub-Antarctic.

Quaternary Science Reviews

Barlow, N.L.M.<sup>1,2\*</sup>, Bentley, M.J.<sup>1</sup>, Spada, G.<sup>3</sup>, Evans, D.J.A.<sup>1</sup>, Hansom, J.D.<sup>4</sup>, Brader, M.D.<sup>1</sup>, White, D.A.<sup>5</sup>,  
Zander, A.<sup>6</sup>, Berg, S.<sup>7</sup>

<sup>1</sup> Department of Geography, Durham University, South Road, Durham, DH1 3LE, UK

<sup>2</sup> School of Earth and Environment, University of Leeds, Leeds, LS2 9JT, UK

<sup>3</sup> Dipartimento di Scienze Pure e Applicate (DiSPeA) Urbino University "Carlo Bo", Urbino, Italy

<sup>4</sup> School of Geographical and Earth Sciences, University of Glasgow, Glasgow, G12 8QQ, UK

<sup>5</sup> Institute for Applied Ecology, University of Canberra, Canberra, ACT 2617, Australia.

<sup>6</sup> Institute of Geography, University of Cologne, Albertus-Magnus-Platz, 50923 Cologne, Germany

<sup>7</sup> Institute of Geology and Mineralogy, University of Cologne, Zùlpicher Str. 49a, 50674 Cologne, Germany

\* Corresponding author: [n.l.m.barlow@leeds.ac.uk](mailto:n.l.m.barlow@leeds.ac.uk) +44 113 343 3761

## **Supplementary information**

### **Database of raised beaches and rock platforms (shown in main text Figure 1): p3-7**

**Table S1:** Raised beach locations and elevations in South Georgia. For references see main text.

**Table S2:** Rock platform locations and elevations in South Georgia. For references see main text.

### **Reports of Enten beach samples and IRSL dating: p8-15**

**Figure S1:** Enten Valley strandplain and IRSL sample locations

**Figure S2:** Site photographs for luminescence samples.

**Tables S3-S4 and Figures S3-S4:** Infra-red stimulated luminescence (IRSL) dating results

### **Report of Little Jason Lagoon Core : p16-18**

**Figure S5:** Site photograph of Little Jason Lagoon

### **GIA modelling : p19**

**Figure S6:** Zoomed in graph of the Holocene highstand portion of the GIA outputs from Figure 8

**Table S1 – Raised beaches**

No.	Location	Latitude	Longitude	Elevation (m)	Source
1	Hamilton Bay	-54.79412	-35.90121	7	Hansom, 1979
2	Cooper Bay	-54.792077	-35.814659	5	This study
3	Cooper Bay	-54.789154	-35.818142	4	This study
4	Cooper Bay	-54.781818	-35.813023	4	Stone, 1976
5	Wirik Bay	-54.751709	-35.845035	5	Stone, 1976
6	Wirik Bay	-54.743355	-35.859795	3	Stone, 1976
7	Iris Bay	-54.696988	-35.930618	9	Stone, 1976
8	Gold Harbour	-54.617414	-35.938819	9	Stone, 1974
9	Bjornstadt Bay	-54.590954	-35.924955	7	Stone, 1974
10	Royal Bay	-54.577820	-35.979003	3	Stone, 1974
11	Royal Bay	-54.567385	-36.016540	8	Stone, 1974
12	Little Moltke Harbour, Royal Bay	-54.548743	-36.105710	4	This study
13	Moltke Harbour, Royal Bay	-54.523322	-36.086989	7	This study
14	Moltke Harbour, Royal Bay	-54.522224	-36.087810	5	This study
15	Molte Harbour, Royal Bay	-54.521123	-36.087053	6	Stone, 1974
16	Molte Harbour, Royal Bay	-54.518153	-36.040411	7	Stone, 1974
17	Sacramento Bight	-54.501913	-36.026061	3	Stone, 1974
18	Kelp Bay, St Andrews Bay	-54.466449	-36.116617	5	Stone, 1974
				7	Gordon and Hansom, 1986;
19	Doris Bay, St Andrews Bay	-54.460396	-36.151381		Stone, 1974
20	Cape Douglas, Barff Peninsula	-54.261184	-36.346232	7	This study
21	Barff Point, Barff Peninsula	-54.245932	-36.400931	6	Stone, 1974
22	Cumberland East Bay	-54.300032	-36.373914	7	This study
23	Sandebugten, Cumberland East Bay	-54.311321	-36.355364	9	Stone, 1974
24	Cumberland East Bay	-54.326764	-36.352630	6	Stone, 1974
25	Cumberland East Bay	-54.338908	-36.346132	7	This study
26	Cumberland East Bay	-54.351525	-36.330976	5	This study

27	Cumberland East Bay	-54.353919	-36.333105	3	This study
28	Cumberland East Bay	-54.356602	-36.339284	3	This study
29	Cumberland East Bay	-54.336905	-36.412918	3	This study
30	Cumberland East Bay	-54.316727	-36.437528	3	This study
31	Moraine Fjord, Cumberland East Bay	-54.316307	-36.446042	2	This study
32	Moraine Fjord, Cumberland East Bay	-54.325379	-36.456353	2	This study
33	King Edward Cove, Cumberland East Bay	-54.292298	-36.492794	5	This study
34	Ocean Harbour, Barff Peninsula	-54.332568	-36.259238	7	Stone, 1974
35	Godthul, Barff Peninsula	-54.292020	-36.307719	3	Stone, 1974
36	Cumberland West Bay	-54.270507	-36.591188	5	This study
37	Harpon Bay, Cumberland West Bay	-54.273448	-36.602583	2	This study
38	Harpon Bay, Cumberland West Bay	-54.275917	-36.601584	3	This study
39	Harpon Bay, Cumberland West Bay	-54.282188	-36.632577	8	Clapperton et al., 1989
40	Harpon Bay, Cumberland West Bay	-54.276308	-36.628343	2	This study
41	Cumberland West Bay	-54.239845	-36.660600	4	This study
42	Carlita Bay, Cumberland West Bay	-54.235723	-36.640279	8	This study
43	Carlita Bay, Cumberland West Bay	-54.239602	-36.634643	4	This study
44	Enten Bay, Cumberland West Bay	-54.213579	-36.612893	5	This study
45	Husvik Harbour, Stromness Bay	-54.190319	-36.679328	5	This study
46	Husvik Harbour, Stromness Bay	-54.185335	-36.706726	7	This study
47	Husvik Harbour, Stromness Bay	-54.183755	-36.707230	7	This study
48	Husvik Harbour, Stromness Bay	-54.181722	-36.708769	7	This study
49	Tonsberg Peninsula, Stromness	-54.165710	-36.659796	7	This study
50	Possession Bay	-54.083352	-37.065312	6	Hansom, 1979
51	Prince Olaf Harbour	-54.065462	-37.134008	7	Hansom, 1979
52	Beckmann Fjord	-54.048199	-37.176948	6	Hansom, 1979
53	Sea Leopard Fjord	-54.076213	-37.230420	3	This study
54	Sea Leopard Fjord	-54.077645	-37.252221	3	This study
55	Salisbury Plain, Bay of Isles	-54.054020	-37.335500	3	This study
56	Ample Bay, Bay of Isles	-54.061210	-37.401926	3	This study

57	Camp Bay, Bay of Isles	-54.038457	-37.445683	6	This study
58	Rosita Harbour, Bay of Isles	-54.020803	-37.450014	6	This study
59	Koppervik, Bay of Isles	-54.006245	-37.407243	3	This study
60	Right Whale Bay	-54.012572	-37.671352	7	Hansom, 1979
61	Narval Bay, Ice Fjord	-54.038574	-37.668930	7	Hansom, 1979
62	Miles Bay, Ice Fjord	-54.077482	-37.644893	8	This study
63	Ice Fjord	-54.087112	-37.699770	6	This study
64	Wilson Harbour	-54.113449	-37.712907	7	This study
65	Wilson Harbour	-54.107989	-37.678074	7	This study
66	Wilson Harbour	-54.115091	-37.643622	10	This study
67	Elephant Cove	-54.162721	-37.682000	3	This study
68	Samuel Islands	-54.186266	-37.619195	6	This study
69	Nilse Hullet	-54.175069	-37.584658	7	This study
70	Cheapman Bay	-54.155831	-37.544184	3	This study
71	Cheapman Bay	-54.152844	-37.559075	3	This study
72	Cheapman Bay	-54.141160	-37.530861	4	This study
73	Larvik	-54.373718	-36.886355	7	Hansom, 1979

**Table S2 – Rock platforms**

<b>No.</b>	<b>Location</b>	<b>Latitude</b>	<b>Longitude</b>	<b>Elevation (m)</b>	<b>Source</b>
1	Shannon Point, Esbensen Bay	-54.870925	-35.969609	30	This study
2	Drgyalski Fjord	-54.814507	-35.926221	30	This study
3	Drgyalski Fjord	-54.814289	-35.914384	30	This study
4	Drgyalski Fjord	-54.811071	-35.912044	30	This study
5	Royal Bay	-54.564990	-35.942405	25	This study
6	Moltke Harbour, Royal Bay	-54.519166	-36.048442	50	Stone, 1974
7	Moltke Harbour, Royal Bay	-54.518537	-36.053162	38	Stone, 1974
8	Moltke Harbour, Royal Bay	-54.518278	-36.059816	25	Stone, 1974
9	Sacramento Bight	-54.503704	-36.022202	52	Clapperton et al., 1989
10	St Andrews Bay	-54.456267	-36.155054	20	This study
11	Kelp Bay, St Andrews Bay	-54.463656	-36.124076	17	This study
12	King Edward Cove, Cumberland East Bay	-54.291335	-36.494657	22	This study
13	Cumberland East Bay	-54.337037	-36.416799	21	This study
14	Cumberland East Bay	-54.316879	-36.434037	12	This study
15	Cape George, Horseshoe Bay	-54.287898	-36.251663	25	Stone, 1974
16	Cumberland West Bay	-54.271738	-36.591302	21	This study
17	Carlita Bay, Cumberland West Bay	-54.239376	-36.646619	24	This study
18	Carlita Bay, Cumberland West Bay	-54.235761	-36.646163	24	This study
19	Carlita Bay, Cumberland West Bay	-54.240930	-36.642994	24	This study
20	Enten Bay, Cumberland West Bay	-54.215899	-36.605693	13	This study
21	Tonsberg Peninsula, Stromness Bay	-54.166759	-36.655650	21	This study
22	Tonsberg Peninsula, Stromness Bay	-54.167279	-36.653791	21	This study
23	Tonsberg Peninsula, Stromness Bay	-54.170185	-36.667705	21	This study
24	Tonsberg Peninsula, Stromness Bay	-54.170364	-36.675168	21	This study
25	Husvik Harbour, Stromness Bay	-54.179827	-36.638004	30	This study
26	Husvik Harbour, Stromness Bay	-54.184856	-36.648625	31	This study
27	Husvik Harbour, Stromness Bay	-54.186770	-36.688748	22	This study

28	Husvik Harbour, Stromness Bay	-54.187178	-36.693433	21	This study
29	Husvik Harbour, Stromness Bay	-54.184923	-36.695271	17	This study
30	Husvik Harbour, Stromness Bay	-54.178185	-36.709810	13	This study
31	Husvik Harbour, Stromness Bay	-54.187625	-36.705893	13	This study

## **Beach and foredune complex in Enten Valley**

Modern and relict beaches were investigated in detail on the northern shore of Cumberland Bay west during the 2013 Polarstern expedition. Here, relict beach sediments were observed to be covered in a layer of fine-coarse sand that had been winnowed from the beaches and transported inland.

At Jason Bay, only one large relict beach complex is present, and Aeolian sands on this raised marine shoreline were dispersed evenly and typically only a few 10's of cm thick. However, at nearby Enten Bay, beach progradation appears to have been much more rapid, and at least seven large beach ridges (E1-7, Figures S1 and S2), and several smaller ridges are preserved across a 400 m wide strandplain. Aeolian sands have built up behind each successive major beach ridge, and in several cases have produced a distinct foredune. The largest, most inland dune in Enten Bay is over two metres thick, and preserves distinct cross stratification that dips inland (Figure S2).

Dunes are typically covered by moss and tussock, while the more gravelly beach faces are commonly dominated by grassy vegetation. Most of the more inland dune sands are indurated and are covered by a thin (0.1-0.3m) layer of peat, with soil and peat thicknesses generally increasing inland, suggesting increasing age. Peat accumulations on the dunes are substantially thinner than on the nearby (near sea level) moraines, which are commonly covered by over a metre of peat, suggesting the beaches post-date the moraines by some time.

A topographic transect across the strandplain (Figure 4) was constructed using a measuring tape ( $\pm 0.05$  m) and sighting clinometer ( $\pm 0.25^\circ$ ) survey along the centreline of the valley, benchmarked to local observations of mean sea level ( $\pm 0.2$  m). Estimated uncertainties for each measured spot elevation (and relative sea level measurement) along the survey transect are  $<0.5$  m. Elevations of samples and the transition from Aeolian sand to beach cobbles were measured relative to the surveyed land surface. The thickness of sand and peat along the surveyed transect was measured where possible using natural sections, and elsewhere by pushing a wooden staff into the sediment until the underlying beach cobbles were intersected.

Infra-Red Stimulated Luminescence (IRSL) samples were collected at four sites, from three major beach ridges (E1, E4 and E7) in Enten Valley. Luminescence samples were collected in from small trenches hand-

dug into natural sections, using 50x300 mm PVC tubes 5-10 cm above the contact between the coarse-grained beach cobbles and the finer dune sands. At least two kilograms of dune sand homogenised from around the tubes was collected for dosimetry using high-resolution gamma ray spectroscopy. Feldspars isolated from the luminescence samples were dated at the University of Cologne using an IR50 Single Aliquot Regeneration (SAR) dose protocol (Tables S2-S4, Figure S4-S5).

The aeolian sediments provide IRSL ages that follow their geomorphic and stratigraphic position. Basal sediments from the thin shadow dunes on the modern beach ridge (E1) provide an IRSL age  $700 \pm 100$  a (131/L-3331). A non-zero age for sample 131 is consistent with the slightly oxidised character of the sampled horizon, and suggests that the luminescence signal of the Aeolian sediments is thoroughly reset (bleached) during littoral reworking on the beach face and/or transport during the short distance to the dune. Duplicate samples on sediment from the same horizon (080a/b), and at different locations (081) on the oldest ridge (E7) provide ages within analytical error, confirming the repeatability of the technique in this environment.

The combined geomorphic-stratigraphic context of the beach sediments provides a record of relative sea level since the formation of the oldest ridge (E7)  $\sim 4,000$  years before present. The beach ridge top produced at this time was  $\sim 5.4$  m above sea level (m asl), at least 3.5 m higher than the modern ridge (E1, 1.7 m asl). Ridge elevations fall sharply to the next major beach ridge (E6) at  $\sim 2.6$  m asl. Elevations of the remaining survey beaches (E2-E4) are likely similar to the modern ridge when survey uncertainties are considered. The limited preservation of ridges at higher elevations, and the similarity in elevation of ridges produced during the last 1200 years (i.e. E1-E4) suggests the rate of relative sea level fall may have been highest immediately after deposition of E7, and has reduced since this time.



Figure S1. Enten Valley strandplain and IRSL sample locations (A) Overview of lower Enten Valley beach ridges. (B, C) insets show location of surveyed transect (yellow dashed line) and major beach ridges (white dotted lines), labelled E1 to E7. (D) detail of relict dune/ridge E7 and sample site 080, note staff (1 m long) and blue figure for scale in the centre-right of the image.



Figure S2. Site photographs for luminescence samples. Aeolian landforms range from small shadow dunes behind tussocks on the modern beach (131) to large foredunes present at ridge E7 (samples 080 and 081). Note the red iron-induration in sections at site 136 and 080, and the distinct cross stratification present at site 080 (east to left). White arrows denote location of luminescence samples. Samples at site 080 were from ~ 2 m below the fur seal.

## Infra-red stimulated luminescence (IRSL) dating results

**Table S3:** Results of high resolution gamma-ray spectrometry, water content determination and calculated dose rates ( $D_0$ ) for coarse grain feldspar samples, including an alpha efficiency of  $0.07 \pm 0.02$  and an internal potassium content of  $12.5 \pm 0.5$  %. The cosmic dose contribution was calculated according to the sampling depth (Prescott and Hutton, 1988; 1994), using the R software package (Kreutzer et al., 2012).

Lab.-code	Sample-ID	Grain size <sup>1</sup> ( $\mu\text{m}$ )	w.c. <sup>2</sup> (weight %)	w.c. <sup>3</sup> (weight %)	Depth (m.b.s)	Dose rate $D_0$ (Gy/ka)	Uranium (ppm)	Thorium (ppm)	Potassium (%)
C-L3328	080a	100-250	18.3	$15 \pm 5$	1.4	$2.38 \pm 0.16$	$1.20 \pm 0.06$	$4.50 \pm 0.26$	$1.24 \pm 0.05$
C-L3329	080b	100-250	15.9	$15 \pm 5$	1.2	$2.42 \pm 0.16$	$1.21 \pm 0.06$	$4.61 \pm 0.27$	$1.27 \pm 0.05$
C-L3330	081	100-250	12.2	$15 \pm 5$	0.4	$2.37 \pm 0.16$	$1.18 \pm 0.06$	$4.50 \pm 0.26$	$1.20 \pm 0.05$
C-L3331	131	100-250	6.1	$10 \pm 5$	0.3	$2.49 \pm 0.16$	$1.20 \pm 0.06$	$4.75 \pm 0.28$	$1.30 \pm 0.01$
C-L3332	136	100-250	14.4	$15 \pm 5$	0.5	$2.46 \pm 0.17$	$1.23 \pm 0.07$	$4.58 \pm 0.28$	$1.28 \pm 0.01$

<sup>1</sup> = potassium feldspars, sample preparation with hydrochloric acid, sodium oxalate and hydrogen peroxide, density separation with sodium polytungstate  $2.58 \text{ g/cm}^3$ .

<sup>2</sup> = water content measured.

<sup>3</sup> = water content used for age calculation.

**Table S4:** Equivalent dose ( $D_e$ ) measurements and IRSL dating results, using a IR50 Single Aliquot Regeneration (SAR) dose protocol and an automated Risø TL/OSL reader (TL-DA-15, Bøtter-Jensen et al., 2003). Measuring details:

Stimulation: Infra-red emitting LEDs ( $880 \Delta 80 \text{ nm}$ ) for 200 s.

Detection: EMI 9235 photomultiplier tube with a L.O.T. Oriel 410 nm interference filter.

Preheat: 10 s at  $210 \text{ }^\circ\text{C}$ , determined by preheat plateau test and dose recovery test (Fig. S1 and S2).

Samples: 8 mm on stainless steel discs, fixed with silicon oil, very low signal intensity.

Lab. Code	Sample ID	OD <sup>1</sup> (%)	RSD <sup>2</sup> (%)	Aliquots <sup>3</sup> (n)	Equivalent dose <sup>4</sup> $D_e$ (Gy)	IRSL age <sup>5</sup> (a)	$g$ -value <sup>6</sup> (%decade <sup>-1</sup> )
C-L3328	080A	11.21	15.60	11/14	9.06±0.58	<b>3810 ± 350</b>	-0.66±0.31
C-L3329	080B	4.70	10.30	21/24	9.65±0.52	<b>3980 ± 340</b>	0.43±0.33
C-L3330	081	14.70	17.40	19/24	10.32±0.64	<b>4350 ± 400</b>	1.0±0.4
C-L3331	131	27.2	31.5	21/31	1.83±0.21	<b>710 ± 100</b>	0.72±0.32
C-L3332	136	15.05	16.48	20/31	2.9±0.18	<b>1180 ± 110</b>	0.94±0.32

<sup>1</sup> = overdispersion.

<sup>2</sup> = relative standard deviation.

<sup>3</sup> = number of accepted and measured subsamples.

<sup>4</sup> = single exponential fitting and central age model (Galbraith et al., 1999).

<sup>5</sup> = not fading corrected since fading rates of 1-1.5 %decade<sup>-1</sup> are most likely artefacts of measurement procedures (Buylaert et al., 2012).

<sup>6</sup> = determined with the model of Lamothe et al. (2003), described by Auclair et al. (2003).

All values are shown with their 1-sigma error and the  $D_e$ -errors include a 5 % uncertainty for the beta source calibration.

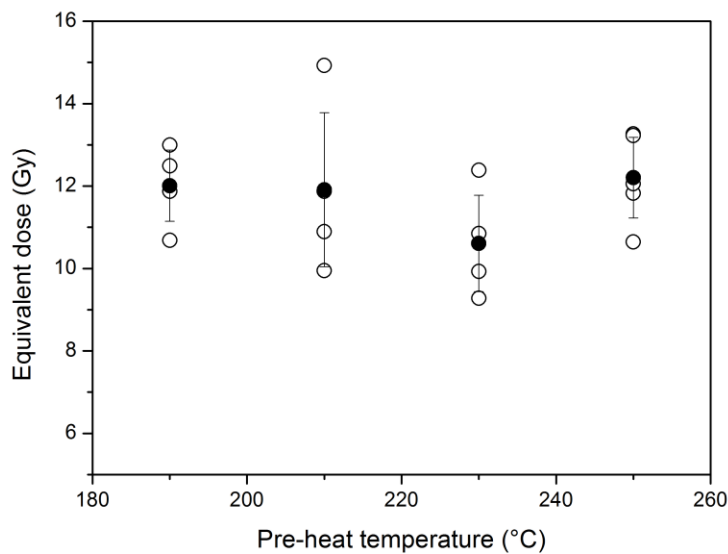


**Figure S3:** Pre-heat plateau of sample 080b, showing individual (open circle) and averaged (filled circle) natural  $De$  values obtained for 10 s pre-heat between 190 °C and 250°C.

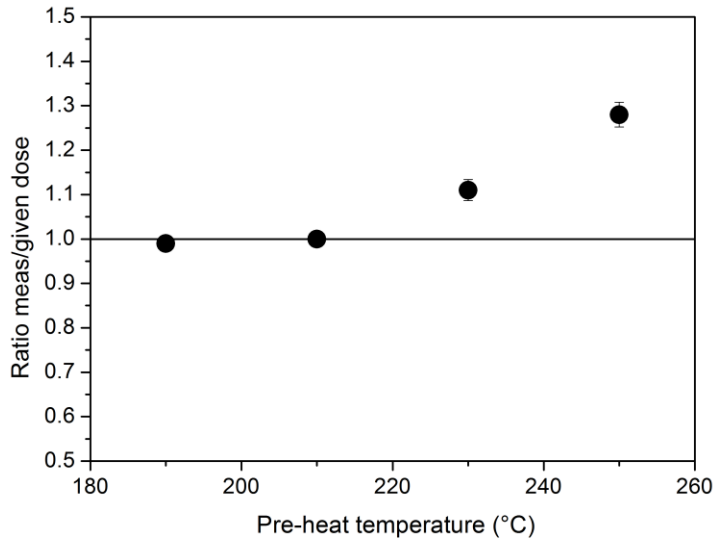


**Figure S4:** Dose recovery pre-heat plateau tests resulted in measured to given dose ratios between 0.96 and 1.00 for the 210 °C pre-heat temperature, indicating a short plateau in the lower temperature range. Sample 081 yielded a measured to given dose ratio of 1.00 after bleaching for 24 hrs in a solar simulator and a beta dose of 27.6 Gy.

## References

- Auclair, M., Lamothe, M., Huot, S., 2003. Measurement of anomalous fading for feldspar IRSL using SAR, *Radiation measurements* 37, 487-492.
- Boetter-Jensen, L., Andersen, C.E., Duller, G.A.T., Murray, A.S., 2003. Developments in irradiation, stimulation and observation facilities in luminescence measurements. *Radiation Measurements* 37, 535-541.
- Buylaert, J.P., Jain, M., Murray, A.S., Thomsen, K.J., Thiel, C. Sohbaty, R., 2012. A robust feldspar luminescence dating method for Middle and Late Pleistocene sediments, *Boreas* 41, 435-451.

- Galbraith, R.F., Roberts, R.G., Laslett, G.M., Yoshida, H., Olley, J.M., 1999. Optical dating of single and multiple grains of quartz from Jinmium Rock Shelter, Northern Australia: part I, Experimental design and statistical models. *Archaeometry* 41, 339-364.
- Huntley, D.J., Lamothe, M., 2001. Ubiquity of anomalous fading in K-feldspars and the measurement and correction for it in optical dating. *Canadian Journal of Earth Science* 38, 1093-1106.
- Kreutzer, S., Schmidt, C., Fuchs, M.C., Dietze, M., Fischer, M., Fuchs, M., 2012. Introducing an R package for luminescence dating analysis. *Ancient TL* 30, 1-8.
- Lamothe, M., Auclair, M., Hamzaoui, C., Huot, S., 2003. Towards a prediction of longterm anomalous fading of feldspar IRSL. *Radiation Measurements* 37, 493-498.
- Prescott, J.R., Hutton, J.T., 1988. Cosmic ray and gamma ray dosimetry for TL and ESR. *Nuclear Tracks and Radiation Measurements* 14, 223-227.
- Prescott, J.R., Hutton, J.T., 1994. Cosmic ray contributions to dose rates for Luminescence and ESR Dating: large depths and long-term variations. *Radiation Measurements*, 23, 497-500.

## Little Jason Lagoon Core

### Study Site

Little Jason Lagoon (LJL) is a coastal inlet on north-eastern side of Cumberland West Bay (54°11.568'S 36°35.469'W; Fig. 1 and S4). Bathymetry of the inlet was surveyed during a field campaign in March 2013 within the scope of expedition ANT XXIX/4 of the RV "Polarstern" (Melles et al. 2013). A sediment core (Co1305) was retrieved in the centre of the lagoon with a piston corer (UWITEK, Austria) from 19.6 m water depth.



**Figure S5:** Little Jason Lagoon, view from Lewin Peninsula towards Cumberland West Bay. Coring location of core Co1305 indicated (after Melles et al. 2013).

### Methods

The sediment core Co1305 was opened in laboratories of the Institute of Geology and Mineralogy of the University of Cologne. For documentation the opened core was photographed using line-scan imaging (GeoTek Co.). For elemental analysis semi-quantitative XRF scans were obtained with an ITRAX XRF core scanner (Cox Ltd.; Croudace et al., 2006). Settings for the analysis with a chromium X-ray tube were 30 mA and 30 kV. The measurement was conducted with an exposure time of 20 sec, and a step-size of 2 mm. Results of the XRF measurement are given as counts per second (cps), which is a semi-quantitative measure of element concentration.

Radiocarbon analysis on macroscopic plant fossils was carried out at the CologneAMS (University of Cologne, Germany). Prior to analysis the material was washed with hydrochloric acid (1% HCl for 10h at room temperature) for decarbonisation and graphitized with an AGE graphitisation system (Wacker et al.

2010). The radiocarbon age has been calibrated with calib rev7.1.0 calibration programme (Stuiver & Reimer 1993) with the SHcal13 dataset (Hogg et al. 2013).

### **Core lithology and results of elemental analysis and radiocarbon dating**

Core Co1305 has a length of 11.04 m. From 10.42 to 9.78 m depth sediments are finely laminated and mainly fine grained (silt and clay). Lamination and generally fine grain sizes point to a low-energy depositional environment. The colour of the sediment is dark greyish/bluish in the lower part and shows a distinct change to brownish/greenish colours above 9.98 m (Figure 5). Sulphur counts indicate incorporation of sulphur in the sediments likely reflecting the production and preservation of organic matter in LJJ. Sulphur concentrations strongly increase between 10.01 cm and 9.98 cm (Figure 5). We interpret this increase in sulphur as a change from lacustrine to brackish/marine conditions. The inflow of seawater into a freshwater environment causes changing redox conditions and can lead to enhanced sulphur fixation (Berg et al. 2010). The transition from a freshwater to marine environment has also been identified on the basis of  $\delta^{13}\text{C}$  of TOC and diatom data (unpublished data). Plant remains, likely mosses, have been found in a sample from 9.94-9.96 m depth, above the transition (Figure 5). Since the mosses are not in situ, but have been transported into the lagoon, the radiocarbon age of these plants (COL2841  $8966 \pm 106$   $^{14}\text{C}$  yr;  $10043 \pm 290$  cal yr BP) gives a maximum age for sedimentation and for the transition from freshwater to marine conditions in LJJ.

### **References**

- Berg, S., Wagner, B., Cremer, H., Leng, M.J., Melles, M. 2010. Late Quaternary environmental and climate history of Rauer Group, East Antarctica. *Palaeogeography Palaeoclimatology Palaeoecology* 297, 201-213.
- Croudace, I.W., Rindby, A., Rothwell, R.G. 2006. ITRAX: description and evaluation of a new multi-function X-ray core scanner. From: Rothwell, R.G. 2006 *New techniques in Sediment Core Analysis*. Geological Society, London, Special Publications 267, 51-63.
- Hogg, A.G., Hua, Q., Blackwell, P.G., Buck, C.E., Guilderson, T.P., Heaton, T.J., Niu, M., Palmer, J.G., Reimer, P.J., Reimer, R.W., Turney, C.S.M., Zimmerman, S.R.H. 2013. Shcal13 southern hemisphere calibration, 0–50,000 years cal BP. *Radiocarbon* 55, 1889-1903.
- Melles, M., Bennike, O., Leng, M., Ritter, B., Viehberg, F., White, D. 2013. Late quaternary climatic and environmental history of South Georgia. *Report on Polar Research* 115-135.
- Stuiver, M., Reimer, P.J., 1993. *Radiocarbon* 35, 215-230.

Wacker, L., Nemec, M., Bourquin, J. 2010. A revolutionary graphitisation system: Fully automated, compact and simple. Nuclear instruments and methods in Physics research B 268, 931-934.

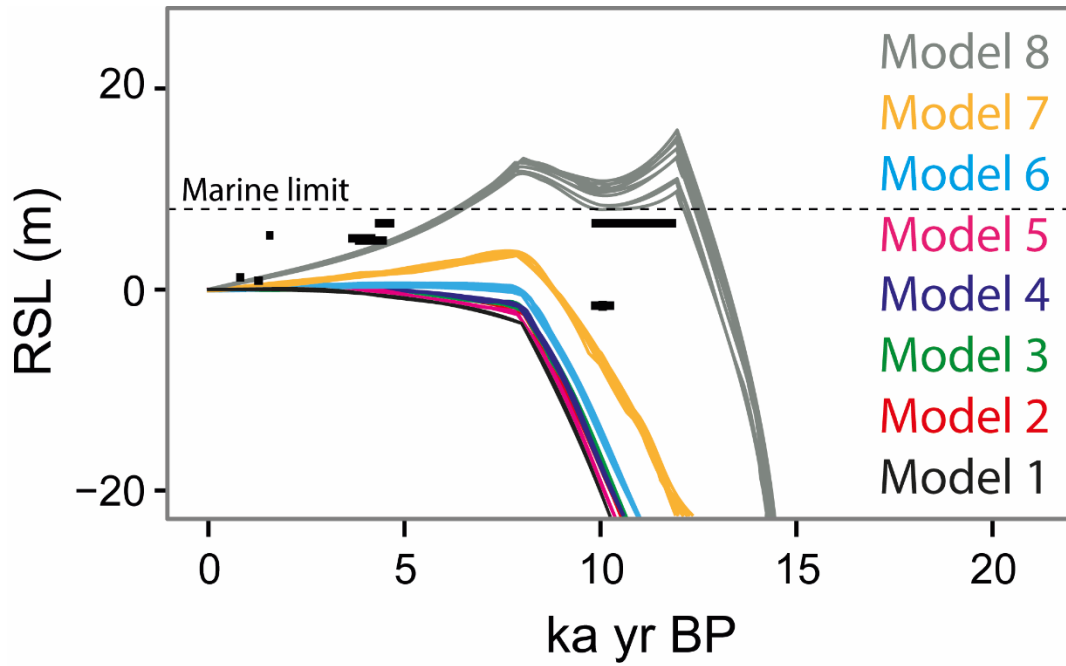


**Figure S6:** Zoomed in graph of the Holocene highstand portion of the GIA outputs from Figure 8. Model numbers as detailed in Table 2.